

Towards the standardization of quantum state verification using optimal strategies

Xinhe Jiang,^{1,*} Kun Wang,^{2,*} Kaiyi Qian,^{1,*} Zhaozhong Chen,^{1,*} Zhiyu Chen,¹
Liangliang Lu,¹ Lijun Xia,¹ Fangmin Song,¹ Shining Zhu,¹ and Xiaosong Ma^{1,†}

¹*National Laboratory of Solid-state Microstructures, School of Physics,
Collaborative Innovation Center of Advanced Microstructures,
State Key Laboratory for Novel Software Technology,
Department of Computer Science and Technology,
Nanjing University, Nanjing 210093, China*

²*Shenzhen Institute for Quantum Science and Engineering, Southern
University of Science and Technology, Shenzhen 518055, China*

Quantum devices for generating entangled states have been extensively studied and widely used. As so, it becomes necessary to verify that these devices truly work reliably and efficiently as they are specified. Here, we experimentally realize the recently proposed two-qubit entangled state verification strategies using both local measurements (nonadaptive) and active feed-forward operations (adaptive) with a photonic platform. About 3283/536 number of copies (N) are required to achieve a 99% confidence to verify the target quantum state for nonadaptive/adaptive strategies. These optimal strategies provide the Heisenberg scaling of the infidelity ϵ as a function of N ($\epsilon \sim N^r$) with the parameter $r = -1$, exceeding the standard quantum limit with $r = -0.5$. We experimentally obtain the scaling parameter of $r = -0.88 \pm 0.03$ and -0.78 ± 0.07 for nonadaptive and adaptive strategies, respectively. Our experimental work could serve as a standardized procedure for the verification of quantum states.

* These authors contributed equally to this work.

† xiaosong.ma@nju.edu.cn

INTRODUCTION

Quantum state plays an important role in quantum information processing.¹ Quantum devices for creating quantum states are building blocks for quantum technology. Being able to verify these quantum states reliably and efficiently is an essential step towards practical applications of quantum devices.² Typically, a quantum device is designed to output some desired state ρ , but the imperfection in the device's construction and noise in the operations may result in the actual output state deviating from it to some random and unknown states σ_i . A standard way to distinguish these two cases is quantum state tomography.³⁻⁷ However, this method is both time-consuming and computationally challenging.^{8,9} Non-tomographic approaches have also been proposed to accomplish the task,¹⁰⁻¹⁷ yet these methods make some assumptions either on the quantum states or on the available operations. It is then natural to ask whether there exists an efficient non-tomographic approach to accomplish the task?

The answer is affirmative. Quantum state verification protocol checks the device's quality efficiently. Various studies have been explored using local measurements.^{14,16,18,19} Some earlier works considered the verification of maximally entangled states.²⁰⁻²³ In the context of hypothesis testing, optimal verification of maximally entangled state is proposed in ref. 20. Under the independent and identically distributed setting, Hayashi et al. discussed the hypothesis testing of the entangled pure states.²³ In a recent work,²⁴ Pallister et al. proposed an optimal strategy to verify non-maximally entangled two-qubit pure states under locally projective and nonadaptive measurements. The locality constraint induces only a constant-factor penalty over the nonlocal strategies. Since then, numerous works have been done along this line of research,²⁵⁻³¹ targeting on different states and measurements. Especially, the optimal verification strategies under local operations and classical communication are proposed recently,²⁷⁻²⁹ which exhibit better efficiency. We also remark related works by Dimić et al.³² and Saggio et al.,³³ in which they developed a generic protocol for efficient entanglement detection using local measurements and with an exponentially growing confidence versus the number of copies of the quantum state.

In this work, we report an experimental two-qubit state verification procedure using both optimal nonadaptive (local measurements) and adaptive (active feed-forward operations) strategies with an optical setup. Compared with previous works merely on minimizing the number of measurement settings,³⁴⁻³⁶ we also minimize the number of copies (i.e., coincidence counts in our experiment) required to verify the quantum state generated by the quantum device. We perform two tasks—Task A and Task B. With Task A, we obtain a fitting infidelity and the number of copies required to achieve a 99% confidence to verify the quantum state. Task B is performed to estimate the confidence parameter δ and infidelity parameter ϵ versus the number of copies N . We experimentally compare the scaling of $\delta-N$ and $\epsilon-N$ by applying the nonadaptive strategy²⁴ and adaptive strategy²⁷⁻²⁹ to the two-qubit states. With our methods, we obtain a comprehensive judgement about the quantum state generated by a quantum device. Present experimental and data analysis workflow may be regarded as a standard procedure for quantum state verification.

RESULTS

Quantum state verification

Consider a quantum device \mathcal{D} designed to produce the two-qubit pure state

$$|\Psi\rangle = \sin\theta|HH\rangle + \cos\theta|VV\rangle, \quad (1)$$

where $\theta \in [0, \pi/4]$. However, it might work incorrectly and actually outputs independent two-qubit fake states $\sigma_1, \sigma_2, \dots, \sigma_N$ in N runs. The goal of the verifier is to determine the fidelity threshold of these fake states to the target state with a certain confidence. We remark that the state for $\theta = \pi/4$ is the maximally entangled state and $\theta = 0$ is the product state. As special cases of the general state in Eq. (1), all the analysis methods presented in the following can be applied to the verification of maximally entangled state and product state. The details of the verification strategies for maximally entangled state and product state are given in Supplementary Notes 1.C and 1.D. Previously, theoretical^{20,23,37} and experimental²¹ works have studied the verification of maximally entangled state. Here, we focus mainly on the verification of non-maximally entangled state in the main text, which is more advantageous in certain experiments comparing to maximally entangled state. For instance, in the context of loophole-free Bell test, non-maximally entangled states require lower detection efficiency than maximally entangled states^{38–41}. The details and experimental results for the verification of maximally entangled state and product state are shown in the Supplementary Notes 2 and 4. To realize the verification of our quantum device, we perform the following two tasks in our experiment (see Fig. 1):

Task A: Performing measurements on the fake states copy by copy according to verification strategy, and make statistics on the number of copies required before we find the first fail event. The concept of Task A is shown in Fig. 1b.

Task B: Performing a fixed number (N) of measurements according to verification strategy, and make statistics on the number of copies that pass the verification tests. The concept of Task B is shown in Fig. 1c.

Task A is based on the assumption that there exists some $\epsilon > 0$ for which the fidelity $\langle\Psi|\sigma_i|\Psi\rangle$ is either 1 or satisfies $\langle\Psi|\sigma_i|\Psi\rangle \leq 1 - \epsilon$ for all $i \in \{1, \dots, N\}$ (see Fig. 1b). Our task is to determine which is the case for the quantum device. To achieve **Task A**, we perform binary-outcome measurements from a set of available projectors to test the state. Each binary-outcome measurement $\{M_l, \mathbb{1} - M_l\}$ ($l = 1, 2, 3, \dots$) is specified by an operator M_l , corresponding to passing the test. For simplicity, we use M_l to denote the corresponding binary measurement. This measurement is performed with probability p_l . We require the target state $|\Psi\rangle$ always passes the test, i.e., $M_l|\Psi\rangle = |\Psi\rangle$. In the bad case ($\langle\Psi|\sigma_i|\Psi\rangle \leq 1 - \epsilon$), the maximal probability that σ_i can pass the test is given by^{24,25}

$$\max_{\langle\Psi|\sigma_i|\Psi\rangle \leq 1 - \epsilon} \text{Tr}(\Omega\sigma_i) = 1 - [1 - \lambda_2(\Omega)]\epsilon := 1 - \Delta_\epsilon, \quad (2)$$

where $\Omega = \sum_l p_l M_l$ is called an strategy, Δ_ϵ is the probability σ_i fails a test and $\lambda_2(\Omega)$ is the second largest eigenvalue of Ω . Whenever σ_i fails the test, we know immediately that the device works incorrectly. After N runs, σ_i in the incorrect case can pass all these tests with probability being at most $[1 - [1 - \lambda_2(\Omega)]\epsilon]^N$. Hence to achieve confidence $1 - \delta$, it suffices to conduct N number of measurements satisfying²⁴

$$N \geq \frac{\ln \delta}{\ln[1 - [1 - \lambda_2(\Omega)]\epsilon]} \approx \frac{1}{[1 - \lambda_2(\Omega)]\epsilon} \ln \frac{1}{\delta}. \quad (3)$$

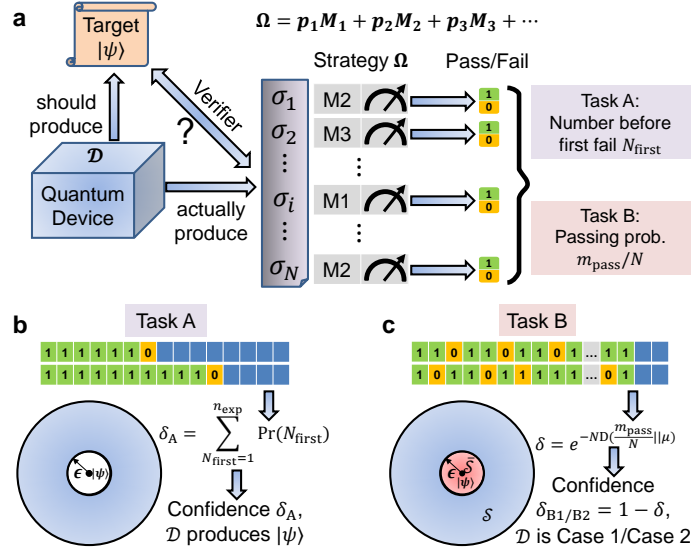


Fig. 1 Illustration of quantum state verification strategy. **a** Consider a quantum device \mathcal{D} designed to produce the two qubit pure state $|\psi\rangle$. However, it might work incorrectly and actually outputs two-qubit fake states $\sigma_1, \sigma_2, \dots, \sigma_N$ in N runs. For each copy σ_i , randomly projective measurements $\{M_1, M_2, M_3, \dots\}$ are performed by the verifier based on their corresponding probabilities $\{p_1, p_2, p_3, \dots\}$. Each measurement outputs a binary outcome 1 for pass and 0 for fail. The verifier takes two tasks based on these measurement outcomes. **b** Task A gives the statistics on the number of copies required before finding the first fail event. From these statistics, the verifier obtains the confidence δ_A that the device outputs state $|\psi\rangle$. **c** Task B performs a fixed number (N) of measurements and makes a statistic on the number of copies (m_{pass}) passing the test. From these statistics, the verifier can judge with a certain confidence δ_{B1}/δ_{B2} that the device belongs to Case 1 or Case 2.

From Eq. (3) we can see that an optimal strategy is obtained by minimizing the second largest eigenvalue $\lambda_2(\Omega)$, with respect to the set of available measurements. Pallister et al.²⁴ proposed an optimal strategy for **Task A**, using only locally projective measurements. Since no classical communication is involved, this strategy (hereafter labelled as Ω_{opt}) is nonadaptive. Later, Wang et al.²⁷, Yu et al.²⁸ and Li et al.²⁹ independently propose the optimal strategy using one-way local operations and classical communication (hereafter labelled as $\Omega_{\text{opt}}^{\rightarrow}$) for two-qubit pure states. Furthermore, Wang et al.²⁷ also gives the optimal strategy for two-way classical communication. The adaptive strategy allows general local operations and classical communication measurements and is shown to be more efficient than the strategies based on local measurements. Thus it is important to realize the adaptive strategy in the experiment. We refer to the Supplementary Notes 1 and 2 for more details on these strategies.

In reality, quantum devices are never perfect. Another practical scenario is to conclude with high confidence that the fidelity of the output states are above or below a certain threshold. To be specific, we want to distinguish the following two cases:

Case 1: \mathcal{D} works correctly – $\forall i, \langle \psi | \sigma_i | \psi \rangle > 1 - \epsilon$. In this case, we regard the device as “good”.

Case 2: \mathcal{D} works incorrectly – $\forall i, \langle \psi | \sigma_i | \psi \rangle \leq 1 - \epsilon$. In this case, we regard the device as “bad”.

We call this **Task B** (see Fig. 1c), which is different from **Task A**, since the condition for ‘ \mathcal{D} works correctly’ is less

restrictive compared with that of **Task A**. It turns out that the verification strategies proposed for **Task A** are readily applicable to **Task B**. Concretely, we perform the nonadaptive verification strategy Ω_{opt} sequentially in N runs and count the number of passing events m_{pass} . Let X_i be a binary variable corresponding to the event that σ_i passes the test ($X_i = 1$) or not ($X_i = 0$). Thus we have $m_{\text{pass}} = \sum_{i=1}^N X_i$. Assume that the device is “good”, then from Eq. (2) we can derive that the passing probability of the generated states is no smaller than $1 - [1 - \lambda_2(\Omega_{\text{opt}})]\epsilon$. We refer to Lemma 3 in the Supplementary Note 3.A for proof. Thus the expectation of X_i satisfies $\mathbb{E}[X_i] \geq 1 - (1 - \lambda_2(\Omega_{\text{opt}}))\epsilon \equiv \mu$. The independence assumption together with the law of large numbers then guarantee $m_{\text{pass}} \geq N\mu$, when N is sufficiently large. We follow the statistical analysis methods using the Chernoff bound in the context of state verification^{28,32,33,42}, which is related to the security analysis of quantum key distributions^{43,44}. We then upper bound the probability that the device works incorrectly as

$$\delta \equiv e^{-N D(\frac{m_{\text{pass}}}{N} \parallel \mu)}, \quad (4)$$

where $D(x \parallel y) := x \log_2 \frac{x}{y} + (1-x) \log_2 \frac{1-x}{1-y}$ is the Kullback-Leibler divergence. That is to say, we can conclude with confidence $\delta_{B1} = 1 - \delta$ that \mathcal{D} belongs to **Case 1**. Conversely, if the device is “bad”, then using the same argument we can conclude with confidence $\delta_{B2} = 1 - \delta$ that \mathcal{D} belongs to **Case 2**. Please refer to the Supplementary Note 3 for rigorous proofs and arguments on how to evaluate the performance of the quantum device for these two cases.

To perform **Task B** with the adaptive strategy $\Omega_{\text{opt}}^{\rightarrow}$, we record the number of passing events $m_{\text{pass}} = \sum_{i=1}^N X_i$. If the device is “good”, the passing probability of the generated states is no smaller than $\mu_s \equiv 1 - [1 - \lambda_4(\Omega_{\text{opt}}^{\rightarrow})]\epsilon$ where $\lambda_4(\Omega_{\text{opt}}^{\rightarrow}) = \sin^2 \theta / (1 + \cos^2 \theta)$ is the smallest eigenvalue of $\Omega_{\text{opt}}^{\rightarrow}$, as proved by Lemma 5 in Supplementary Note 3.B. The independence assumption along with the law of large numbers guarantee that $m_{\text{pass}} \geq N\mu_s$, when N is sufficiently large. On the other hand, if the device is “bad”, we can prove that the passing probability of the generated states is no larger than $\mu_l \equiv 1 - [1 - \lambda_2(\Omega_{\text{opt}}^{\rightarrow})]\epsilon$, where $\lambda_2(\Omega_{\text{opt}}^{\rightarrow}) = \cos^2 \theta / (1 + \cos^2 \theta)$, by Lemma 4 in Supplementary Note 3.B. Again, the independence assumption and the law of large numbers guarantee that $m_{\text{pass}} \leq N\mu_l$, when N is large enough. Therefore, we consider two regions regarding the value of m_{pass} in the adaptive strategy, i.e., the region $m_{\text{pass}} \leq N\mu_s$ and the region $m_{\text{pass}} \geq N\mu_l$. In these regions, we can conclude with $\delta_{B1} = 1 - \delta_l / \delta_{B2} = 1 - \delta_s$ that the device belongs to **Case 1/Case 2**. The expressions for δ_l and δ_s and all the details for applying adaptive strategy to **Task B** can be found in Supplementary Note 3.B.

Experimental setup and verification procedure

Our two-qubit entangled state is generated based on a type-II spontaneous parametric down-conversion in a 20 mm-long periodically-poled potassium titanyl phosphate (PPKTP) crystal, embedded in a Sagnac interferometer^{45,46} (see Fig. 2). A continuous-wave external-cavity ultraviolet (UV) diode laser at 405 nm is used as the pump light. A half-wave plate (HWP1) and quarter-wave plate (QWP1) transform the linear polarized light into the appropriate elliptically polarized light to provide the power balance and phase control of the pump field. With an input pump power of ~ 30 mW, we typically obtain 120 kHz coincidence counts.

The target state has the following form

$$|\psi\rangle = \sin \theta |HV\rangle + e^{i\phi} \cos \theta |VH\rangle, \quad (5)$$

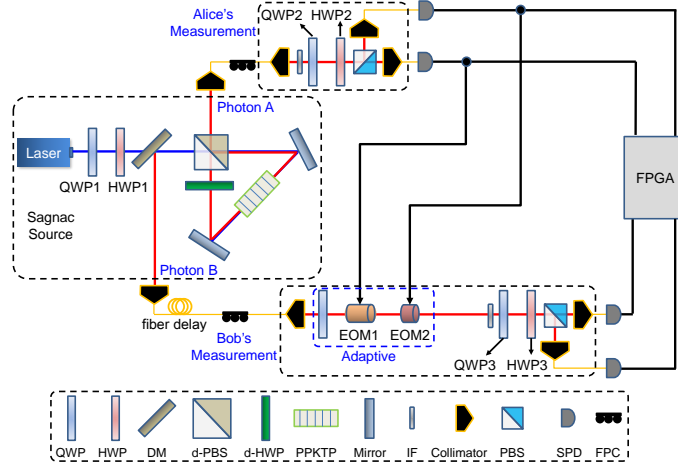


Fig. 2 Experimental setup for optimal verification of two-qubit quantum state. We use a photon pair source based on a Sagnac interferometer to generate various two-qubit quantum state. QWP1 and HWP1 are used for adjusting the relative amplitude of the two counter-propagating pump light. For nonadaptive strategy, the measurement is realized with QWP, HWP and polarizing beam splitter (PBS) at both Alice's and Bob's site. The adaptive measurement is implemented by real-time feed-forward operation of electro-optic modulators (EOMs), which are triggered by the detection signals recorded with a field-programmable gate array (FPGA). The optical fiber delay is used to compensate the electronic delay from Alice's single photon detector (SPD) to the two EOMs. QWP: quarter-wave plate; HWP: half-wave plate; DM: Dichroic mirror; PBS: polarizing beam splitter; IF: 3-nm interference filter centered at 810 nm; dPBS: dual-wavelength polarizing beam splitter; dHWP: dual-wavelength half-wave plate; PPKTP: periodically poled KTiOPO₄; FPC: Fiber polarization controller.

where θ and ϕ represent amplitude and phase, respectively. This state is locally equivalent to $|\Psi\rangle$ in Eq. (1) by $U = \begin{pmatrix} 1 & 0 \\ 0 & 1 \end{pmatrix} \otimes \begin{pmatrix} 0 & e^{i\phi} \\ 1 & 0 \end{pmatrix}$. By using Lemma 1 in Supplementary Note 1, the optimal strategy for verifying $|\psi\rangle$ is $\Omega'_{\text{opt}} = U\Omega_{\text{opt}}U^\dagger$, where Ω_{opt} is the optimal strategy verifying $|\Psi\rangle$ in Eq. (1). In the Supplementary Note 2, we write down explicitly the optimal nonadaptive strategy²⁴ and adaptive strategy^{27–29} for verifying $|\psi\rangle$.

In our experiment, we implement both the nonadaptive and adaptive measurements to realize the verification strategies. There are four settings $\{P_0, P_1, P_2, P_3\}$ for nonadaptive measurements²⁴ while only three settings $\{\tilde{T}_0, \tilde{T}_1, \tilde{T}_2\}$ are required for the adaptive measurements.^{27–29} The exact form of these projectors is given in the Supplementary Note 2. Note that the measurements $P_0 = \tilde{T}_0 = |H\rangle\langle H| \otimes |V\rangle\langle V| + |V\rangle\langle V| \otimes |H\rangle\langle H|$ are determined by the standard σ_z basis for both the nonadaptive and adaptive strategies, which are orthogonal and can be realized with a combination of QWP, HWP and polarization beam splitter (PBS). For adaptive measurements, the measurement bases $\tilde{v}_+ = e^{i\phi} \cos\theta|H\rangle + \sin\theta|V\rangle$ / $\tilde{w}_+ = e^{i\phi} \cos\theta|H\rangle - i \sin\theta|V\rangle$ and $\tilde{v}_- = e^{i\phi} \cos\theta|H\rangle - \sin\theta|V\rangle$ / $\tilde{w}_- = e^{i\phi} \cos\theta|H\rangle + i \sin\theta|V\rangle$ at Bob's site are not orthogonal. Note that we only implement the one-way adaptive strategy in our experiment. The two-way adaptive strategy is also derived in ref. 27. Compared to nonadaptive and one-way adaptive strategy, the two-way adaptive strategy gives improvements on the verification efficiency due to the utilization of more classical communication resources. The implementation of two-way adaptive strategy requires: First, Alice performs her measurement and sends her results to Bob; Then, Bob performs his measurement

according to Alice's outcomes; Finally, Alice performs another measurement conditioning on Bob's measurement outcomes. This procedure requires the real-time communications both from Alice to Bob and from Bob to Alice. Besides, the two-way adaptive strategy requires the quantum nondemolition measurement at Alice's site, which is difficult to implement in the current setup. To realize the one-way adaptive strategy, we transmit the results of Alice's measurements to Bob through classical communication channel, which is implemented by real-time feed-forward operations of the electro-optic modulators (EOMs). As shown in Fig. 2, we trigger two EOMs at Bob's site to realize the adaptive measurements based on the results of Alice's measurement. If Alice's outcome is $|+\rangle = (|V\rangle + |H\rangle)/\sqrt{2}$ or $|R\rangle = (|V\rangle + i|H\rangle)/\sqrt{2}$, EOM1 implement the required rotation and EOM2 is identity operation. Conversely, if Alice's outcome is $|-\rangle = (|V\rangle - |H\rangle)/\sqrt{2}$ or $|L\rangle = (|V\rangle - i|H\rangle)/\sqrt{2}$, EOM2 will implement the required rotation and EOM1 is identity operation. Our verification procedure is the following.

(1) Specifications of quantum device. We adjust the HWP1 and QWP1 of our Sagnac source to generate the desired quantum state.

(2) Verification using the optimal strategy. In this stage, we generate many copies of the quantum state sequentially with our Sagnac source. These copies are termed as fake states $\{\sigma_i, i = 1, 2, \dots, N\}$. Then, we perform the optimal nonadaptive verification strategy to σ_i . From the parameters θ and ϕ of target state, we can compute the angles of wave plates QWP2 and HWP2, QWP3 and HWP3 for realizing the projectors $\{P_0, P_1, P_2, P_3\}$ required in the nonadaptive strategy. To implement the adaptive strategy, we employ two EOMs to realize the \tilde{v}_+/\tilde{v}_- and \tilde{w}_+/\tilde{w}_- measurements once receiving Alice's results (refer to Supplementary Note 2.B for the details). Finally, we obtain the timetag data of the photon detection from the field programmable gate array (FPGA) and extract individual coincidence count (CC) which is regarded as one copy of our target state. We use the timetag experimental technique to record the channel and arrival time of each detected photon for data processing.⁴⁷ The time is stored as multiples of the internal time resolution (~ 156 ps). The first data in the timetag is recorded as the starting time t_{i0} . With the increasing of time, we search the required CC between different channels within a fixed coincidence window (0.4 ns). If a single CC is obtained, we record the time of the ended timetag data as t_{f0} . Then we move to the next time slice $t_{i1}-t_{f1}$ to search for the next CC. This process can be cycled until we find the N -th CC in time slice $t_{iN-1}-t_{fN-1}$. This measurement can be viewed as single-shot measurement of the bipartite state with post-selection. The time interval in each slice is about 100 μ s in our experiment, consistent with the $1/\text{CR}$, CR-coincidence rate. By doing so, we can precisely obtain the number of copies N satisfying the verification requirements. We believe this procedure is suitable in the context of verification protocol, because one wants to verify the quantum state with the minimum amount of copies.

(3) Data processing. From the measured timetag data, the results for different measurement settings can be obtained. For the nonadaptive strategy, $\{P_0, P_1, P_2, P_3\}$ are chosen randomly with the probabilities $\{\mu_0, \mu_1, \mu_2, \mu_3\}$ ($\mu_0=\alpha(\theta)$, $\mu_i=(1-\alpha(\theta))/3$) with $\alpha(\theta) = (2 - \sin(2\theta))/(4 + \sin(2\theta))$. For the adaptive strategy, $\{\tilde{T}_0, \tilde{T}_1, \tilde{T}_2\}$ projectors are randomly chosen according to the probabilities $\{\beta(\theta), (1 - \beta(\theta))/2, (1 - \beta(\theta))/2\}$, where $\beta(\theta) = \cos^2 \theta/(1 + \cos^2 \theta)$. For **Task A**, we use CC to decide whether the outcome of each measurement is pass or fail for each σ_i . The passing

probabilities for the nonadaptive strategy can be, respectively, expressed as,

$$P_0 : \frac{CC_{HV} + CC_{VH}}{CC_{HH} + CC_{HV} + CC_{VH} + CC_{VV}}, \quad (6)$$

$$P_i : \frac{CC_{\tilde{u}_i \tilde{v}_i^\perp} + CC_{\tilde{u}_i^\perp \tilde{v}_i} + CC_{\tilde{u}_i^\perp \tilde{v}_i^\perp}}{CC_{\tilde{u}_i \tilde{v}_i} + CC_{\tilde{u}_i \tilde{v}_i^\perp} + CC_{\tilde{u}_i^\perp \tilde{v}_i} + CC_{\tilde{u}_i^\perp \tilde{v}_i^\perp}}. \quad (7)$$

where $i = 1, 2, 3$, and $\tilde{u}_i/\tilde{u}_i^\perp$ and $\tilde{v}_i/\tilde{v}_i^\perp$ are the orthogonal bases for each photon and their expressions are given in the Supplementary Note 2.A. For P_0 , if the individual CC is in CC_{HV} or CC_{VH} , it indicates that σ_i passes the test and we set $X_i = 1$; otherwise, it fails to pass the test and we set $X_i = 0$. For P_i , $i = 1, 2, 3$, if the individual CC is in $CC_{\tilde{u}_i \tilde{v}_i^\perp}$, $CC_{\tilde{u}_i^\perp \tilde{v}_i}$ or $CC_{\tilde{u}_i^\perp \tilde{v}_i^\perp}$, it indicates that σ_i passes the test and we set $X_i = 1$; otherwise, it fails to pass the test and we set $X_i = 0$. For the adaptive strategy, we set the value of the random variables X_i in a similar way.

We increase the number of copies (N) to decide the occurrence of the first failure for **Task A** and the frequency of passing events for **Task B**. From these data, we obtain the relationship of the confidence parameter δ , the infidelity parameter ϵ , and the number of copies N . There are certain probabilities that the verifier fail for each measurement. In the worst case, the probability that the verifier fails to assert σ_i is given by $1 - \Delta_\epsilon$, where $\Delta_\epsilon = 1 - \epsilon/(2 + \sin \theta \cos \theta)$ for nonadaptive strategy²⁴ and $\Delta_\epsilon = 1 - \epsilon/(2 - \sin^2 \theta)$ for adaptive strategy.²⁷⁻²⁹

Results and analysis of two-qubit optimal verification

The target state to be verified is the general two-qubit state in Eq. (5), where the parameter $\theta = k * \pi/10$ and ϕ is optimized with maximum likelihood estimation method. In this section, we present the results of $k = 2$ state (termed as k2, see Supplementary Note 2) as an example. The verification results of other states, such as the maximally entangled state and the product state, are presented in Supplementary Note 4. Our theoretical non-maximally target state is specified by $\theta = 0.6283$ ($k = 2$). In experiment, we obtain $|\psi\rangle = 0.5987|HV\rangle + 0.8010e^{3.2034i}|VH\rangle$ ($\theta = 0.6419$, $\phi = 3.2034$) as our target state to be verified. In order to realize the verification strategy, the projective measurement is performed sequentially by randomly choosing the projectors. We take 10000 rounds for a fixed 6000 number of copies.

Task A. According to this verification task, we make a statistical analysis on the number of measurements required for the first occurrence of failure. According to the geometric distribution, the probability that the n -th measurement (out of n measurements) is the first failure is

$$\Pr(N_{\text{first}} = n) = (1 - \Delta_\epsilon)^{n-1} \cdot \Delta_\epsilon \quad (8)$$

where $n = 1, 2, 3, \dots$. We then obtain the cumulative probability

$$\delta_A = \sum_{N_{\text{first}}=1}^{n_{\text{exp}}} \Pr(N_{\text{first}}) \quad (9)$$

which is the confidence of the device generating the target state $|\psi\rangle$. In Fig. 3a, we show the distribution of the number N_{first} required before the first failure for the nonadaptive (Non) strategy. From the figure we can see that N_{first} obeys the geometric distribution. We fit the distribution with the function in Eq. (8) and obtain an experimental infidelity $\epsilon_{\text{exp}}^{\text{Non}} = 0.0034(15)$, which is a quantitative estimation of the infidelity for the generated state. From the experimental

statistics, we obtain the number $n_{\text{exp}}^{\text{Non}}=3283$ required to achieve the 99% confidence (i.e., 99% cumulative probability for $N_{\text{first}} \leq n_{\text{exp}}^{\text{Non}}$) of judging the generated states to be the target state in the nonadaptive strategy.

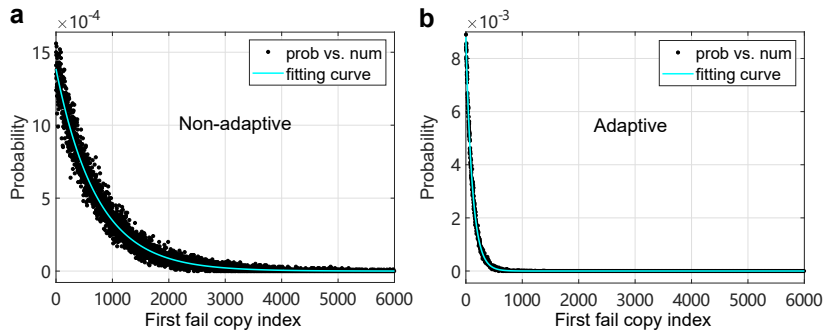


Fig. 3 The distribution of the number required before the first failure. **a** for the nonadaptive strategy. **b** for the adaptive strategy. From the statistics, we obtain the fitting infidelity of $\epsilon_{\text{exp}}^{\text{Non}} = 0.0034(15)$ and $\epsilon_{\text{exp}}^{\text{Adp}} = 0.0121(6)$. The numbers required to achieve a 99% confidence are $n_{\text{exp}}^{\text{Non}}=3283$ and $n_{\text{exp}}^{\text{Adp}}=536$, respectively.

The results for the adaptive (Adp) verification of **Task A** are shown in Fig. 3b. The experimental fitting infidelity for this distribution is $\epsilon_{\text{exp}}^{\text{Adp}} = 0.0121(6)$. The number required to achieve the same 99% confidence as the nonadaptive strategy is $n_{\text{exp}}^{\text{Adp}}=536$. Note this nearly six times (i.e., $n_{\text{exp}}^{\text{Non}}/n_{\text{exp}}^{\text{Adp}} \sim 6$) difference of the experimental number required to obtain the 99% confidence is partially because the infidelity with adaptive strategy is approximately four times larger than the nonadaptive strategy. However, the number of copies required to achieve the same confidence by using the adaptive strategy is still about two times fewer than the nonadaptive strategy even if the infidelity of the generated states is the same, see the analysis presented in Supplementary Note 5. This indicates that the adaptive strategy requires a significant lower number of copies to conclude the device output state $|\psi\rangle$ with 99% confidence compared with the nonadaptive one.

Task B. We emphasize that Task B is considered under the assumption that the quantum device is either in Case 1 or in Case 2 as described above. These two cases are complementary and the confidence to assert whether the device belongs to Case 1 or Case 2 can be obtained according to different values of m_{pass} . We refer to the Supplementary Note 3 for detailed information on judging the quantum device for these two cases. For each case, we can reduce the parameter δ by increasing the number of copies of the quantum state. Thus, the confidence $\delta_{\text{B}} = 1 - \delta$ to judge the device belongs to **Case 1/Case 2** is obtained. For the nonadaptive strategy, the passing probability m_{pass}/N can finally reach a stable value 0.9986 ± 0.0002 after about 1000 number of copies (see Supplementary Note 6). This value is smaller than the desired passing probability μ when we choose the infidelity ϵ_{min} to be 0.001. In this situation, we conclude the state belongs to **Case 2**. Conversely, the stable value is larger than the desired passing probability μ when we choose the infidelity ϵ_{max} to be 0.006. In this situation, we conclude the state belongs to **Case 1**. In Fig. 4, we present the results for the verification of **Task B**. First, we show the the confidence parameter δ versus the number of copies for the nonadaptive strategy in Fig. 4a, b. With about 6000 copies of quantum state, the δ parameter reaches 0.01 for **Case 2**. This indicates that the device belongs to **Case 1** with probability at most 0.01. In other words, there are at least 99% confidence that we can say the device is in ‘bad’ case after about 6000 measurements.

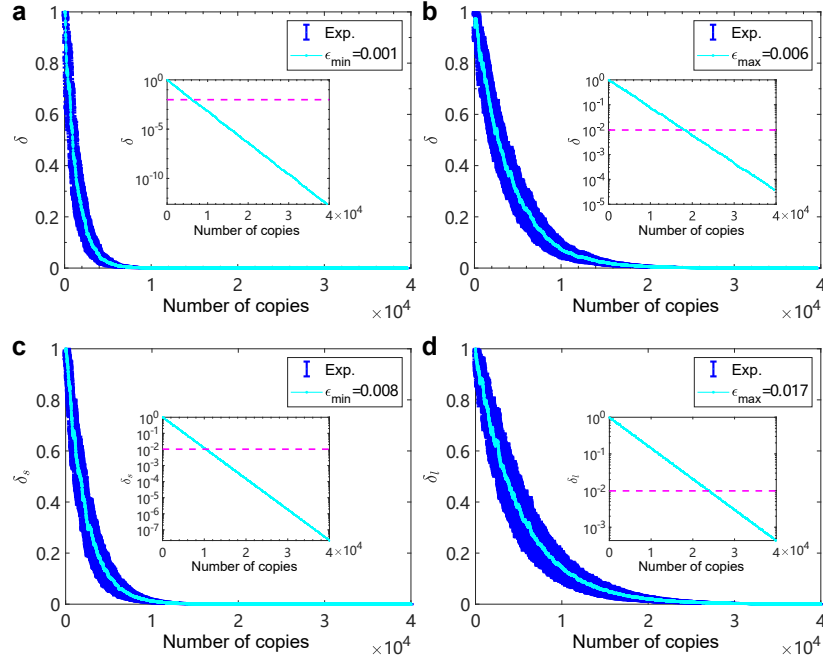


Fig. 4 Experimental results for the verification of Task B. **a,b** Nonadaptive strategy. The confidence parameter δ decreases with the increase of number of copies. After about 6000 copies, δ goes below 0.01 for **Case 2** (see inset of **a**). For **Case 1** (see inset of **b**), it takes about 17905 copies to reduce δ below 0.01. **c,d** Adaptive strategy. The number of copies required to reduce δ_s and δ_l to be 0.01 for the two cases are about 10429 and 23645, respectively. Generally, it takes less number of copies for verifying **Case 2** because more space are allowed for the states to be found in the $0-\mu N$ region. The blue is the experimental error bar (Exp.), which is obtained by 100 rounds of measurements for each coincidence. The insets show the log-scale plots, which indicates δ can reach a value below 0.01 with about thousands to tens of thousands of copies.

Generally, more copies of quantum states are required to reach a same level $\delta=0.01$ for **Case 1**, because there are fewer portion for the number of passing events m_{pass} to be chosen in the range of μN to N . From Fig. 4b, we can see that it takes about 17905 copies of quantum state in order to reduce the parameter δ to be below 0.01. At this stage, we can say that the device belongs to **Case 2** with probability at most 0.01. That is, there are at least 99% confidence that we can say the device is in ‘good’ case after about 17905 measurements.

Figure 4c, d are the results of adaptive strategy. For the adaptive strategy, the passing probability m_{pass}/N finally reaches a stable value 0.9914 ± 0.0005 (see Supplementary Note 6), which is smaller than the nonadaptive measurement due to the limited fidelity of the EOMs’ modulation. Correspondingly, the infidelity parameter for the two cases are chosen to be $\epsilon_{\min} = 0.008$ and $\epsilon_{\max} = 0.017$, respectively. We can see from the figure that it takes about 10429 number of copies for δ_s to be decreased to 0.01 when choosing ϵ_{\min} , which indicates that the device belongs to **Case 2** with at least 99% confidence after about 10429 measurements. On the other hand, about 23645 number of copies are needed for δ_l to be decreased to 0.01 when choosing ϵ_{\max} , which indicates that the device belongs to **Case 1** with at least 99% confidence after about 23645 measurements. Note that the difference of adaptive and nonadaptive comes from the different descent speed of δ versus the number of copies N , which results from the differences in passing probabilities and the infidelity parameters. See Supplementary Note 6 for detailed explanations.

From another perspective, we can fix δ and see how the parameter ϵ changes when increasing the number of copies. Figure 5 presents the variation of ϵ versus the number of copies in the log-log scale when we set the δ to be 0.10. At small number of copies, the infidelity is large and drops fast to a low level when the number of copies increases to be approximately 100. The decline becomes slow when the number of copies exceeds 100. It should be noted that the ϵ asymptotically tends to a value of 0.0036 (calculated by $1 - \Delta_\epsilon = 0.9986$) and 0.012 (calculated by $1 - \Delta_\epsilon = 0.9914$) for the nonadaptive and adaptive strategies, respectively. Therefore, we are still in the region of $m_{\text{pass}}/N \geq \mu$. We can also see that the scaling of ϵ versus N is linear in the small number of copies region. We fit the data in the linear region with $\epsilon \sim N^r$ and obtain a slope $r \sim -0.88 \pm 0.03$ for nonadaptive strategy and $r \sim -0.78 \pm 0.07$ for adaptive strategy. This scaling exceeds the standard quantum limit $\epsilon \sim N^{-0.5}$ scaling^{42,48} for physical parameter estimation. Thus, our method is better for estimating the infidelity parameter ϵ than the classical metrology. Note that m_{pass}/N is a good estimation for our state fidelity. If the state fidelity increases, the slope of linear region will decrease to the Heisenberg limit $\epsilon \sim N^{-1}$ in quantum metrology (see Supplementary Note 6).

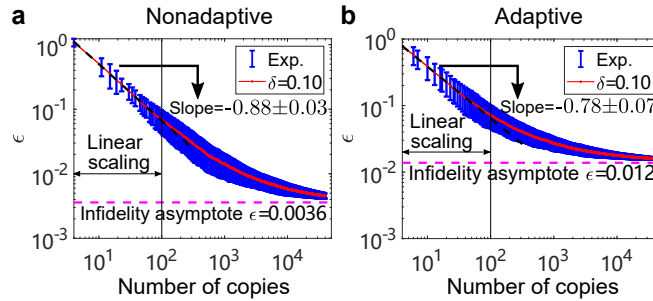


Fig. 5 The variation of infidelity parameter versus the number of copies. **a** Nonadaptive strategy and **b** Adaptive strategy. Here the data is plotted on a log-log scale. The confidence parameter δ is chosen to be 0.10. The parameter ϵ fast decays to a low value which is asymptotically close to the infidelity 0.0036 (Nonadaptive) and 0.012 (Adaptive) of the generated quantum state when increasing the number of copies. The fitting slopes for the linear scaling region are -0.88 ± 0.03 and -0.78 ± 0.07 for the nonadaptive and adaptive, respectively. The blue symbol is the experimental data with error bar (Exp.), which is obtained by 100 rounds of measurements for each coincidence.

Comparison with standard quantum state tomography

The advantage of the optimal verification strategy lies in that it requires fewer number of measurement settings, and more importantly, the number of copies to estimate the quantum states generated by a quantum device. In standard quantum state tomography,⁴⁹ the minimum number of settings required for a complete reconstruction of the density matrix is 3^n , where n is the number of qubits. For two-qubit system, the standard tomography will cost nine settings whereas the present verification strategy only needs four and three measurement settings for the nonadaptive and adaptive strategies, respectively. To quantitatively compare the verification strategy with the standard tomography, we show the scaling of the parameters δ and ϵ versus the number of copies N in Fig. 6. For each number of copies, the fidelity estimation $F \pm \Delta F$ can be obtained by the standard quantum state tomography. The δ of standard tomography is calculated by the confidence assuming normal distribution of the fidelity with mean F and standard

deviation ΔF . The ϵ of standard tomography is calculated by $\epsilon = 1 - F$. The result of verification strategy is taken from the data in Figs. 4 and 5 for the nonadaptive strategy. For δ versus N , we fit the curve with equation $\delta = e^{g \cdot N}$, where g is the scaling of $\log(\delta)$ with N . We obtain $g_{\text{tomo}} = -6.84 \times 10^{-5}$ for the standard tomography and $g_{\text{verif}} = -7.35 \times 10^{-4}$ for the verification strategy. This indicates that present verification strategy achieves better confidence than standard quantum state tomography given the same number of copies. For ϵ versus N , as shown in Fig. 6b, the standard tomography will finally reach a saturation value when increasing the number of copies. With the same number of copies N , the verification strategy obtains a smaller ϵ , which indicates that the verification strategy can give a better estimation for the state fidelity than the standard quantum state tomography when small number of quantum states are available for a quantum device.

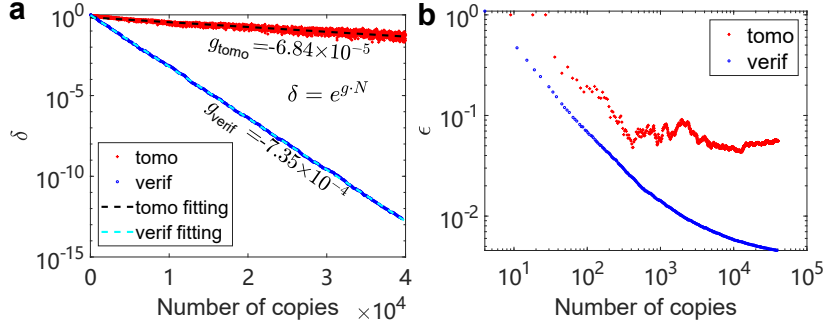


Fig. 6 Comparison of standard quantum state tomography and present verification strategy. In the figure, we give the variation of **a** δ and **b** ϵ versus the number of copies N by using standard quantum state tomography (tomo) and present verification strategy (verif). For standard tomography, the fidelity $F \pm \Delta F$ is first obtained from the reconstructed density matrix of each copy N . Then confidence parameter δ is estimated by assuming normal distribution of the fidelity with mean F and standard deviation ΔF . The infidelity parameter ϵ is estimated by $\epsilon = 1 - F$. Note that the experimental data symbols shown in **a** looks like lines due to the dense data points.

DISCUSSION

Our work, including experiment, data processing and analysis framework, can be used as a standardized procedure for verifying quantum states. In Task A, we give an estimation of the infidelity parameter ϵ_{exp} of the generated states and the confidence δ_A to produce the target quantum state by detecting certain number of copies. With the ϵ_{exp} obtained from Task A, we can choose ϵ_{max} or ϵ_{min} which divides our device to be Case 1 or Case 2. Task B is performed based on the chosen ϵ_{min} and ϵ_{max} . We can have an estimation for the scaling of the confidence parameter δ versus the number of copies N based on the analysis method of Task B. With a chosen δ , we can also have an estimation for the scaling of the infidelity parameter ϵ versus N . With these steps, we can have a comprehensive judgement about how well our device really works.

In summary, we report experimental demonstrations for the optimal two-qubit pure state verification strategy with and without adaptive measurements. We give a clear discrimination and comprehensive analysis for the quantum states generated by a quantum device. Two tasks are proposed for practical applications of the verification strategy. The variation of confidence and infidelity parameter with the number of copies for the generated quantum states are

presented. The obtained experimental results are in good agreement with the theoretical predictions. Furthermore, our experimental framework offers a precise estimation on the reliability and stability of quantum devices. This ability enables our framework to serve as a standard tool for analysing quantum devices. Our experimental framework can also be extended to other platforms.

DATA AVAILABILITY

The data that support the plots within this paper and other findings of this study are available from the corresponding author upon reasonable request.

CODE AVAILABILITY

The codes that support the plots within this paper and other findings of this study are available from the corresponding author upon reasonable request.

ACKNOWLEDGEMENTS

The authors thank B. Dakić for the helpful discussions. This work was supported by the National Key Research and Development Program of China (Nos. 2017YFA0303704 and 2019YFA0308704), the National Natural Science Foundation of China (Nos. 11674170 and 11690032), NSFC-BRICS (No. 61961146001), the Natural Science Foundation of Jiangsu Province (No. BK20170010), the Leading-edge technology Program of Jiangsu Natural Science Foundation (No. BK20192001), the program for Innovative Talents and Entrepreneur in Jiangsu, and the Fundamental Research Funds for the Central Universities.

COMPETING INTERESTS

A patent application related to this work is filed by Nanjing University on 29 May, 2020 in China. The application number is 202010475173.4 (Patent in China). The status of the application is now under patent pending.

AUTHOR CONTRIBUTIONS

X.-H. J., K.-Y. Q., Z.-Z. C., Z.-Y. C. and X.-S. M. designed and performed the experiment. K. W. performed the theoretical analysis. X.-H. J., K.-Y. Q. analysed the data. X.-H. J., K. W. and X.-S. M. wrote the paper with input from all authors. All authors discussed the results and read the manuscript. F.-M. S., S.-N. Z. and X.-S. M. supervised the work. X.-H. J., K. W., K.-Y. Q., Z.-Z. C. contributed equally to this work.

REFERENCES

1. Nielsen, M. A. & Chuang, I. L. *Quantum Computation and Quantum Information* (Cambridge University Press, UK, 2010).
2. Paris, M. & Rehacek, J. *Quantum state estimation*, vol. 649 (Springer Science & Business Media, 2004).
3. Sugiyama, T., Turner, P. S. & Muraio, M. Precision-guaranteed quantum tomography. *Phys. Rev. Lett.* **111**, 160406 (2013).
4. Gross, D., Liu, Y.-K., Flammia, S. T., Becker, S. & Eisert, J. Quantum state tomography via compressed sensing. *Phys. Rev. Lett.* **105**, 150401 (2010).
5. Haah, J., Harrow, A. W., Ji, Z., Wu, X. & Yu, N. Sample-optimal tomography of quantum states. In *Proceedings of the Forty-eighth Annual ACM Symposium on Theory of Computing*, STOC 2016, 913–925 (ACM, New York, NY, USA, 2016).
6. Donnell, R. & Wright, J. Efficient quantum tomography. In *Proceedings of the 48th Annual ACM Symposium on Theory of Computing*, STOC 2016, 899–912 (ACM, New York, NY, USA, 2016).
7. Donnell, R. & Wright, J. Efficient quantum tomography II. In *Proceedings of the 49th Annual ACM SIGACT Symposium on Theory of Computing*, STOC 2017, 962–974 (ACM, New York, NY, USA, 2017).
8. Häffner, H. *et al.* Scalable multiparticle entanglement of trapped ions. *Nature* **438**, 643–646 (2005).
9. Carolan, J. *et al.* On the experimental verification of quantum complexity in linear optics. *Nature Photon.* **8**, 621–626 (2014).
10. Tóth, G. & Gühne, O. Detecting genuine multipartite entanglement with two local measurements. *Phys. Rev. Lett.* **94**, 060501 (2005).
11. Flammia, S. T. & Liu, Y.-K. Direct fidelity estimation from few Pauli measurements. *Phys. Rev. Lett.* **106**, 230501 (2011).
12. da Silva, M. P., Landon-Cardinal, O. & Poulin, D. Practical characterization of quantum devices without tomography. *Phys. Rev. Lett.* **107**, 210404 (2011).
13. Aolita, L., Gogolin, C., Kliesch, M. & Eisert, J. Reliable quantum certification of photonic state preparations. *Nature Commun.* **6**, 8498 (2015).
14. Hayashi, M. & Morimae, T. Verifiable measurement-only blind quantum computing with stabilizer testing. *Phys. Rev. Lett.* **115**, 220502 (2015).
15. McCutcheon, W. *et al.* Experimental verification of multipartite entanglement in quantum networks. *Nature Commun.* **7**, 13251 (2016).
16. Takeuchi, Y. & Morimae, T. Verification of many-qubit states. *Phys. Rev. X* **8**, 021060 (2018).
17. Bădescu, C., Donnell, R. & Wright, J. Quantum state certification. In *Proceedings of the 51st Annual ACM SIGACT Symposium on Theory of Computing*, STOC 2019, 503–514 (ACM, New York, NY, USA, 2019).
18. Morimae, T., Takeuchi, Y. & Hayashi, M. Verification of hypergraph states. *Phys. Rev. A* **96**, 062321 (2017).
19. Takeuchi, Y., Mantri, A., Morimae, T., Mizutani, A. & Fitzsimons, J. F. Resource-efficient verification of quantum computing using Serfling’s bound. *npj Quantum Information* **5**, 27 (2019).
20. Hayashi, M., Matsumoto, K. & Tsuda, Y. A study of LOCC-detection of a maximally entangled state using hypothesis testing. *J. Phys. A: Math. Gen.* **39**, 14427–14446 (2006).
21. Hayashi, M. *et al.* Hypothesis testing for an entangled state produced by spontaneous parametric down-conversion. *Phys. Rev. A* **74**, 062321 (2006).
22. Hayashi, M., Tomita, A. & Matsumoto, K. Statistical analysis of testing of an entangled state based on the Poisson distribution framework. *New J. Phys.* **10**, 043029 (2008).
23. Hayashi, M. Group theoretical study of LOCC-detection of maximally entangled states using hypothesis testing. *New J. Phys.* **11**, 043028 (2009).
24. Pallister, S., Linden, N. & Montanaro, A. Optimal verification of entangled states with local measurements. *Phys. Rev. Lett.* **120**, 170502 (2018).

25. Zhu, H. & Hayashi, M. Efficient verification of hypergraph states. *Phys. Rev. Applied* **12**, 054047 (2019).
26. Zhu, H. & Hayashi, M. Efficient verification of pure quantum states in the adversarial scenario. *Phys. Rev. Lett.* **123**, 260504 (2019).
27. Wang, K. & Hayashi, M. Optimal verification of two-qubit pure states. *Phys. Rev. A* **100**, 032315 (2019).
28. Yu, X.-D., Shang, J. & Gühne, O. Optimal verification of general bipartite pure states. *npj Quantum Information* **5**, 112 (2019).
29. Li, Z., Han, Y.-G. & Zhu, H. Efficient verification of bipartite pure states. *Phys. Rev. A* **100**, 032316 (2019).
30. Liu, Y.-C., Yu, X.-D., Shang, J., Zhu, H. & Zhang, X. Efficient verification of Dicke states. *Phys. Rev. Applied* **12**, 044020 (2019).
31. Li, Z., Han, Y.-G. & Zhu, H. Optimal verification of Greenberger-Horne-Zeilinger states. *Phys. Rev. Applied* **13**, 054002 (2020).
32. Dimić, A. & Dakić, B. Single-copy entanglement detection. *npj Quantum Information* **4**, 11 (2018).
33. Saggio, V. *et al.* Experimental few-copy multipartite entanglement detection. *Nature Phys.* **15**, 935–940 (2019).
34. Knips, L., Schwemmer, C., Klein, N., Wieśniak, M. & Weinfurter, H. Multipartite entanglement detection with minimal effort. *Phys. Rev. Lett.* **117**, 210504 (2016).
35. Bavaresco, J. *et al.* Measurements in two bases are sufficient for certifying high-dimensional entanglement. *Nature Phys.* **14**, 1032–1037 (2018).
36. Friis, N., Vitagliano, G., Malik, M. & Huber, M. Entanglement certification from theory to experiment. *Nat. Rev. Phys.* **1**, 72–87 (2019).
37. Zhu, H. & Hayashi, M. Optimal verification and fidelity estimation of maximally entangled states. *Phys. Rev. A* **99**, 052346 (2019).
38. Eberhard, P. H. Background level and counter efficiencies required for a loophole-free Einstein-Podolsky-Rosen experiment. *Phys. Rev. A* **47**, R747–R750 (1993).
39. Giustina, M. *et al.* Bell violation using entangled photons without the fair-sampling assumption. *Nature* **497**, 227–230 (2013).
40. Giustina, M. *et al.* Significant-loophole-free test of Bell’s theorem with entangled photons. *Phys. Rev. Lett.* **115**, 250401 (2015).
41. Shalm, L. K. *et al.* Strong loophole-free test of local realism. *Phys. Rev. Lett.* **115**, 250402 (2015).
42. Zhang, W.-H. *et al.* Experimental optimal verification of entangled states using local measurements. *Phys. Rev. Lett.* **125**, 030506 (2020).
43. Scarani, V. *et al.* The security of practical quantum key distribution. *Rev. Mod. Phys.* **81**, 1301–1350 (2009).
44. Hayashi, M. & Nakayama, R. Security analysis of the decoy method with the Bennett–Brassard 1984 protocol for finite key lengths. *New J. Phys.* **16**, 063009 (2014).
45. Kim, T., Fiorentino, M. & Wong, F. N. C. Phase-stable source of polarization-entangled photons using a polarization Sagnac interferometer. *Phys. Rev. A* **73**, 012316 (2006).
46. Fedrizzi, A., Herbst, T., Poppe, A., Jennewein, T. & Zeilinger, A. A wavelength-tunable fiber-coupled source of narrowband entangled photons. *Opt. Express* **15**, 15377–15386 (2007).
47. UQDevices. Time tag and logic user manual (Last accessed: Version 2.1). URL <https://uqdevices.com/documentation/>. (2017).
48. Giovannetti, V., Lloyd, S. & Maccone, L. Advances in quantum metrology. *Nature Photon.* **5**, 222–229 (2011).

49. Altepeter, J. B., Jeffrey, E. R. & Kwiat, P. Photonic state tomography. vol. 52 of *Advances In Atomic, Molecular, and Optical Physics*, 105–159 (Academic Press, 2005).

Supplementary Information – Towards the standardization of quantum state verification using optimal strategies

Supplementary Note 1. THE THEORY OF OPTIMAL STATE VERIFICATION

First we argue that it suffices to derive optimal verification strategies for the state $|\Psi\rangle$ defined in Eq. (1) of the main text. This is because locally unitarily equivalent pure states have locally unitarily equivalent optimal verification strategies. This fact is proved in ref.¹ (Lemma 2) and we restate here for completeness.

Lemma 1 (Lemma 2 in the Supplemental Material of ref.¹). *Given any two-qubit state $|\psi\rangle$ with optimal strategy Ω , a locally unitarily equivalent state $(U \otimes V)|\psi\rangle$, where U and V are unitaries, has optimal strategy $(U \otimes V)\Omega(U \otimes V)^\dagger$.*

A. Optimal nonadaptive strategy

In this section, we briefly summarize the optimal nonadaptive strategy. According to ref.¹, any optimal strategy for verifying state the state $|\Psi\rangle$ ($\theta \in (0, \pi/4)$) defined in Eq. (1) of the main text, that accepts $|\Psi\rangle$ with certainty and satisfies the properties of locality, projectivity, and trusty, can be expressed as a strategy involving the following four measurements,

$$\Omega_{\text{opt}} = \alpha(\theta)P_{ZZ}^+ + \frac{1 - \alpha(\theta)}{3} \sum_{k=1}^3 [\mathbb{1} - |u_k\rangle\langle u_k| \otimes |v_k\rangle\langle v_k|], \quad (1)$$

where $\alpha(\theta) = (2 - \sin(2\theta))/(4 + \sin(2\theta))$, $P_{ZZ}^+ = |HH\rangle\langle HH| + |VV\rangle\langle VV|$ is the projector onto the positive eigenspace of the tensor product of Pauli matrix $Z \otimes Z$, and the states $\{|u_k\rangle\}$ and $\{|v_k\rangle\}$ are written explicitly in the following:

$$|u_1\rangle = \frac{1}{\sqrt{1 + \tan\theta}}|H\rangle + \frac{e^{\frac{2\pi i}{3}}}{\sqrt{1 + \cot\theta}}|V\rangle, \quad (2)$$

$$|v_1\rangle = \frac{1}{\sqrt{1 + \tan\theta}}|H\rangle + \frac{e^{\frac{\pi i}{3}}}{\sqrt{1 + \cot\theta}}|V\rangle, \quad (3)$$

$$|u_2\rangle = \frac{1}{\sqrt{1 + \tan\theta}}|H\rangle + \frac{e^{\frac{4\pi i}{3}}}{\sqrt{1 + \cot\theta}}|V\rangle, \quad (4)$$

$$|v_2\rangle = \frac{1}{\sqrt{1 + \tan\theta}}|H\rangle + \frac{e^{\frac{5\pi i}{3}}}{\sqrt{1 + \cot\theta}}|V\rangle, \quad (5)$$

$$|u_3\rangle = \frac{1}{\sqrt{1 + \tan\theta}}|H\rangle + \frac{1}{\sqrt{1 + \cot\theta}}|V\rangle, \quad (6)$$

$$|v_3\rangle = \frac{1}{\sqrt{1 + \tan\theta}}|H\rangle - \frac{1}{\sqrt{1 + \cot\theta}}|V\rangle. \quad (7)$$

Correspondingly, the second largest eigenvalue of Ω_{opt} is given by

$$\lambda_2(\Omega_{\text{opt}}) = \frac{2 + \sin(2\theta)}{4 + \sin(2\theta)}. \quad (8)$$

Substitute this value into Eq. (3) of the main text, we find the optimal number of measurements required to verify $|\Psi\rangle$ with infidelity ϵ and confidence $1 - \delta$ satisfies

$$n_{\text{opt}} \approx \frac{1}{[1 - \lambda_2(\Omega_{\text{opt}})]\epsilon} \ln \frac{1}{\delta} = (2 + \sin \theta \cos \theta) \frac{1}{\epsilon} \ln \frac{1}{\delta}. \quad (9)$$

For analysis, we consider the spectral decomposition of Ω_{opt} . This decomposition is helpful for computing the passing probability of the states being verified. Let $|\Psi^\perp\rangle := \cos \theta |HH\rangle - \sin \theta |VV\rangle$. One can check that $\{|\Psi\rangle, |\Psi^\perp\rangle, |HV\rangle, |VH\rangle\}$ forms an orthonormal basis of a two-qubit space. The spectral decomposition of Ω_{opt} is

$$\Omega_{\text{opt}} = |\Psi\rangle\langle\Psi| + \lambda_2(\Omega_{\text{opt}}) (|\Psi^\perp\rangle\langle\Psi^\perp| + |VH\rangle\langle VH| + |HV\rangle\langle HV|), \quad (10)$$

where $\lambda_2(\Omega_{\text{opt}})$ is given in Eq. (8).

B. Optimal adaptive strategy using one-way classical communication

In this section, we briefly summarize the optimal adaptive strategy using one-way classical communication. According to ref.² any optimal strategy for verifying the state $|\Psi\rangle$ ($\theta \in (0, \pi/4)$) defined in Eq. (1) of the main text, that accepts $|\Psi\rangle$ and can be implemented by local measurements together with one-way classical communication, can be expressed as a strategy involving the following three measurements,

$$\Omega_{\text{opt}}^{\rightarrow} = \beta(\theta) P_{ZZ}^+ + \frac{1 - \beta(\theta)}{2} T_1 + \frac{1 - \beta(\theta)}{2} T_2, \quad (11)$$

where $\beta(\theta) = \cos^2 \theta / (1 + \cos^2 \theta)$ and

$$T_1 = |+\rangle\langle+| \otimes |v_+\rangle\langle v_+| + |-\rangle\langle-| \otimes |v_-\rangle\langle v_-|, \quad (12)$$

$$T_2 = |R\rangle\langle R| \otimes |w_+\rangle\langle w_+| + |L\rangle\langle L| \otimes |w_-\rangle\langle w_-|, \quad (13)$$

such that

$$|+\rangle = \frac{|V\rangle + |H\rangle}{\sqrt{2}}, \quad |-\rangle = \frac{|V\rangle - |H\rangle}{\sqrt{2}}, \quad (14)$$

$$|v_+\rangle = \cos \theta |V\rangle + \sin \theta |H\rangle, \quad |v_-\rangle = \cos \theta |V\rangle - \sin \theta |H\rangle, \quad (15)$$

$$|R\rangle = \frac{|V\rangle + i|H\rangle}{\sqrt{2}}, \quad |L\rangle = \frac{|V\rangle - i|H\rangle}{\sqrt{2}}, \quad (16)$$

$$|w_+\rangle = \cos \theta |V\rangle - i \sin \theta |H\rangle, \quad |w_-\rangle = \cos \theta |V\rangle + i \sin \theta |H\rangle. \quad (17)$$

Correspondingly, the second largest eigenvalue of $\Omega_{\text{opt}}^{\rightarrow}$ is given by

$$\lambda_2(\Omega_{\text{opt}}^{\rightarrow}) = \frac{\cos^2 \theta}{1 + \cos^2 \theta}. \quad (18)$$

Substitute this value into Eq. (3) of the main text, we find the optimal number of measurements required to verify $|\Psi\rangle$ with infidelity ϵ and confidence $1 - \delta$ satisfies

$$n_{\text{opt}}^{\rightarrow} \approx \frac{1}{[1 - \lambda_2(\Omega_{\text{opt}}^{\rightarrow})]\epsilon} \ln \frac{1}{\delta} = (1 + \cos^2 \theta) \frac{1}{\epsilon} \ln \frac{1}{\delta}. \quad (19)$$

The spectral decomposition of $\Omega_{\text{opt}}^{\rightarrow}$ is given by

$$\Omega_{\text{opt}}^{\rightarrow} = |\Psi\rangle\langle\Psi| + \lambda_2(\Omega_{\text{opt}}^{\rightarrow}) (|\Psi^{\perp}\rangle\langle\Psi^{\perp}| + |HV\rangle\langle HV|) + \lambda_4(\Omega_{\text{opt}}^{\rightarrow})|VH\rangle\langle VH|, \quad (20)$$

where $\lambda_2(\Omega_{\text{opt}}^{\rightarrow})$ is the second largest eigenvalue given in Eq. (18) and $\lambda_4(\Omega_{\text{opt}}^{\rightarrow}) = \sin^2\theta/(1 + \cos^2\theta)$ is the fourth (which is also the smallest) eigenvalue of $\Omega_{\text{opt}}^{\rightarrow}$.

C. Optimal verification of Bell state

As pointed out in ref.¹, the above nonadaptive strategy is actually only optimal for $\theta \in (0, \pi/4) \cup (\pi/4, \pi/2)$. That is to say, it is no longer optimal for verifying the Bell state, for which $\theta = \pi/4$. In this section, we summary explicitly the optimal strategy for verifying the Bell state of the following form:

$$|\Phi^+\rangle = \frac{1}{\sqrt{2}} (|HH\rangle + |VV\rangle). \quad (21)$$

The first proposal for testing the Bell state $|\Phi^+\rangle$ is given in ref.³. According to Section 7.1 of ref.³ and Eq. (8) of ref.¹, the optimal strategy for verifying $|\Phi^+\rangle$ implementable by locally projective measurements, can be expressed as a strategy involving the following three measurements,

$$\Omega_{\text{opt,Bell}} = \frac{1}{3} (P_{XX}^+ + P_{YY}^- + P_{ZZ}^+), \quad (22)$$

where P_{XX}^+ is the projector onto the positive eigenspace of the tensor product of Pauli matrix $X \otimes X$ and P_{YY}^- is the projector onto the negative eigenspace of the tensor product of Pauli matrix $Y \otimes Y$, similarly defined as that of P_{ZZ}^+ . We can check that $\lambda_2(\Omega_{\text{opt,Bell}}) = 1/3$ and thus the optimal number of measurements required to verify $|\Phi^+\rangle$ with infidelity ϵ and confidence $1 - \delta$ satisfies

$$n_{\text{opt,Bell}} \approx \frac{1}{[1 - \lambda_2(\Omega_{\text{opt,Bell}})]\epsilon} \ln \frac{1}{\delta} = \frac{3}{2\epsilon} \ln \frac{1}{\delta}. \quad (23)$$

D. Optimal verification of a product state

For the product state $|HV\rangle$ ($\theta = 0$ or $\pi/2$), the optimal strategy is provably given by $\Omega_{\text{opt,pd}} = |HV\rangle\langle HV|$. Obviously, $\lambda_2(\Omega_{\text{opt,pd}}) = 1$ and thus the optimal number of measurements required to verify $|HV\rangle$ with infidelity ϵ and confidence $1 - \delta$ satisfies

$$n_{\text{opt,pd}} \approx \frac{1}{[1 - \lambda_2(\Omega_{\text{opt,pd}})]\epsilon} \ln \frac{1}{\delta} = \frac{1}{\epsilon} \ln \frac{1}{\delta}. \quad (24)$$

Supplementary Note 2. THE EXPERIMENT OF OPTIMAL STATE VERIFICATION

A. The verification strategies for experimentally generated state

In our experiment setting, the target state has the form

$$|\psi(\theta, \phi)\rangle = \sin\theta|HV\rangle + e^{i\phi} \cos\theta|VH\rangle, \quad (25)$$

where $\theta \in [0, \pi/4]$ and $\phi \in [0, 2\pi]$, which will be determined by the experimental data. We can see that $|\psi(\theta, \phi)\rangle$ is equivalent to $|\Psi\rangle$ defined in Eq. (1) of the main text through the following unitary operator:

$$\mathbb{U} \equiv (\mathbb{1} \otimes \kappa) = \begin{pmatrix} 1 & 0 \\ 0 & 1 \end{pmatrix} \otimes \begin{pmatrix} 0 & e^{i\phi} \\ 1 & 0 \end{pmatrix}. \quad (26)$$

This is indeed the case since

$$(\mathbb{1} \otimes \kappa)|\Psi\rangle = \begin{pmatrix} 0 & e^{i\phi} & 0 & 0 \\ 1 & 0 & 0 & 0 \\ 0 & 0 & 0 & e^{i\phi} \\ 0 & 0 & 1 & 0 \end{pmatrix} \begin{pmatrix} \sin\theta \\ 0 \\ 0 \\ \cos\theta \end{pmatrix} = \begin{pmatrix} 0 \\ \sin\theta \\ e^{i\phi} \cos\theta \\ 0 \end{pmatrix} = |\psi(\theta, \phi)\rangle. \quad (27)$$

Then Lemma 1 together with the optimal strategies for verifying $|\Psi\rangle$ summarized in the last section yields the optimal strategies for verifying $|\psi(\theta, \phi)\rangle$. For completeness, we write down explicitly the measurements of these strategies.

Optimal nonadaptive strategy for $|\psi(\theta, \phi)\rangle$. By Lemma 1 and Eq. (1), the optimal nonadaptive strategy for verifying $|\psi(\theta, \phi)\rangle$ has the following form,

$$\Omega'_{\text{opt}} = \mathbb{U}\Omega_{\text{opt}}\mathbb{U}^\dagger = \alpha(\theta)P_0 + \frac{1-\alpha(\theta)}{3}(P_1 + P_2 + P_3), \quad (28)$$

where

$$P_0 = \mathbb{U}P_{ZZ}^+\mathbb{U}^\dagger = |H\rangle\langle H| \otimes |V\rangle\langle V| + |V\rangle\langle V| \otimes |H\rangle\langle H|, \quad (29)$$

and P_i for $i = 1, 2, 3$ satisfies $P_i = |\tilde{u}_i\rangle\langle\tilde{u}_i| \otimes |\tilde{v}_i\rangle\langle\tilde{v}_i|$ such that

$$|\tilde{u}_1\rangle = |u_1\rangle = \frac{1}{\sqrt{1+\tan\theta}}|H\rangle + \frac{e^{\frac{2\pi i}{3}}}{\sqrt{1+\cot\theta}}|V\rangle, \quad (30)$$

$$|\tilde{v}_1\rangle = \kappa|v_1\rangle = \frac{1}{\sqrt{1+\tan\theta}}|V\rangle + \frac{e^{\frac{\pi i}{3}}e^{i\phi}}{\sqrt{1+\cot\theta}}|H\rangle, \quad (31)$$

$$|\tilde{u}_2\rangle = |u_2\rangle = \frac{1}{\sqrt{1+\tan\theta}}|H\rangle + \frac{e^{\frac{4\pi i}{3}}}{\sqrt{1+\cot\theta}}|V\rangle, \quad (32)$$

$$|\tilde{v}_2\rangle = \kappa|v_2\rangle = \frac{1}{\sqrt{1+\tan\theta}}|V\rangle + \frac{e^{\frac{5\pi i}{3}}e^{i\phi}}{\sqrt{1+\cot\theta}}|H\rangle, \quad (33)$$

$$|\tilde{u}_3\rangle = |u_3\rangle = \frac{1}{\sqrt{1+\tan\theta}}|H\rangle + \frac{1}{\sqrt{1+\cot\theta}}|V\rangle, \quad (34)$$

$$|\tilde{v}_3\rangle = \kappa|v_3\rangle = \frac{1}{\sqrt{1+\tan\theta}}|V\rangle + \frac{e^{\frac{3\pi i}{3}}e^{i\phi}}{\sqrt{1+\cot\theta}}|H\rangle. \quad (35)$$

Optimal adaptive strategy using one-way classical communication for $|\psi(\theta, \phi)\rangle$. By Lemma 1 and Eq. (11), the optimal adaptive strategy for verifying $|\psi(\theta, \phi)\rangle$, when one-way classical communication is allowed, has the following form,

$$\Omega'_{\text{opt}} \rightarrow \beta(\theta)\tilde{T}_0 + \frac{1-\beta(\theta)}{2}\tilde{T}_1 + \frac{1-\beta(\theta)}{2}\tilde{T}_2, \quad (36)$$

where

$$\tilde{T}_0 = \mathbb{U}P_{ZZ}^+\mathbb{U}^\dagger = |H\rangle\langle H| \otimes |V\rangle\langle V| + |V\rangle\langle V| \otimes |H\rangle\langle H|, \quad (37)$$

$$\begin{aligned} \tilde{T}_1 &= \mathbb{U}T_1\mathbb{U}^\dagger \\ &= |+\rangle\langle +| \otimes \kappa|v_+\rangle\langle v_+|\kappa^\dagger + |-\rangle\langle -| \otimes \kappa|v_-\rangle\langle v_-|\kappa^\dagger \\ &\equiv |+\rangle\langle +| \otimes |\tilde{v}_+\rangle\langle \tilde{v}_+| + |-\rangle\langle -| \otimes |\tilde{v}_-\rangle\langle \tilde{v}_-|, \end{aligned} \quad (38)$$

$$\begin{aligned} \tilde{T}_2 &= \mathbb{U}T_2\mathbb{U}^\dagger \\ &= |R\rangle\langle R| \otimes \kappa|w_+\rangle\langle w_+|\kappa^\dagger + |L\rangle\langle L| \otimes \kappa|w_-\rangle\langle w_-|\kappa^\dagger \\ &\equiv |R\rangle\langle R| \otimes |\tilde{w}_+\rangle\langle \tilde{w}_+| + |L\rangle\langle L| \otimes |\tilde{w}_-\rangle\langle \tilde{w}_-|, \end{aligned} \quad (39)$$

and

$$|+\rangle = \frac{|V\rangle + |H\rangle}{\sqrt{2}}, \quad |-\rangle = \frac{|V\rangle - |H\rangle}{\sqrt{2}}, \quad (40)$$

$$|R\rangle = \frac{|V\rangle + i|H\rangle}{\sqrt{2}}, \quad |L\rangle = \frac{|V\rangle - i|H\rangle}{\sqrt{2}}, \quad (41)$$

$$|\tilde{v}_+\rangle = \kappa|v_+\rangle = e^{i\phi} \cos \theta |H\rangle + \sin \theta |V\rangle, \quad |\tilde{v}_-\rangle = \kappa|v_-\rangle = e^{i\phi} \cos \theta |H\rangle - \sin \theta |V\rangle, \quad (42)$$

$$|\tilde{w}_+\rangle = \kappa|w_+\rangle = e^{i\phi} \cos \theta |H\rangle - i \sin \theta |V\rangle, \quad |\tilde{w}_-\rangle = \kappa|w_-\rangle = e^{i\phi} \cos \theta |H\rangle + i \sin \theta |V\rangle. \quad (43)$$

Experimental optimal verification of Bell state. Experimentally, our target Bell state has the following form

$$|\Phi^-\rangle = \frac{1}{\sqrt{2}} (|HV\rangle - |VH\rangle), \quad (44)$$

which is locally unitarily equivalent to the Bell state $|\Phi^+\rangle$ defined in Eq. (21) through

$$(\mathbb{1} \otimes XZ)|\Psi^+\rangle = \frac{1}{\sqrt{2}} (\mathbb{1} \otimes XZ) (|HH\rangle + |VV\rangle) = \frac{1}{\sqrt{2}} (|HV\rangle - |VH\rangle) = |\Phi^-\rangle. \quad (45)$$

By Lemma 1, the optimal adaptive strategy for verifying $|\Phi^-\rangle$ is given by

$$\Omega'_{\text{opt,Bell}} = \frac{1}{3} (M_1 + M_2 + M_3), \quad (46)$$

where

$$M_1 = (\mathbb{1} \otimes XZ)P_{XX}^+(\mathbb{1} \otimes XZ)^\dagger = |-\rangle\langle -| \otimes |+\rangle\langle +| + |+\rangle\langle +| \otimes |-\rangle\langle -|, \quad (47)$$

$$M_2 = (\mathbb{1} \otimes XZ)P_{YY}^-(\mathbb{1} \otimes XZ)^\dagger = |L\rangle\langle L| \otimes |R\rangle\langle R| + |R\rangle\langle R| \otimes |L\rangle\langle L|, \quad (48)$$

$$M_3 = (\mathbb{1} \otimes XZ)P_{ZZ}^+(\mathbb{1} \otimes XZ)^\dagger = |H\rangle\langle H| \otimes |V\rangle\langle V| + |V\rangle\langle V| \otimes |H\rangle\langle H|. \quad (49)$$

In the above derivation, we have used the following relations:

$$XZ|H\rangle = |V\rangle, \quad XZ|V\rangle = -|H\rangle, \quad (50)$$

$$XZ|+\rangle = -|+\rangle, \quad XZ|-\rangle = |+\rangle, \quad (51)$$

$$XZ|L\rangle = -i|L\rangle, \quad XZ|R\rangle = i|R\rangle. \quad (52)$$

B. The experimental verification procedure

We now describe the procedure on how to verify the states $|\psi(\theta, \phi)\rangle$ described above. The parameter θ and ϕ can be chosen to generate arbitrary pure states according to the angles of our wave plate (QWP1 and HWP1 in Fig. 2 of the main text). In order to tune the angle θ to generate several states between 0 and $\pi/2$, we let $\theta = k \cdot \pi/10$ ($k = 1, 2, 3, 4$). For reference, we list the tomographic parameters for $k = 2$ (k2), maximally entangled state (Max) and product state (HV) used in this article in Supplementary Table 1.

Supplementary Table 1 Target states verified in our experiment.

k	$k\pi/10$	θ	ϕ	Fidelity	Passing Prob. m_{pass}/N
k2	0.6283	0.6419	3.2034	0.9964±0.0002	0.9986±0.0002
Max	$\pi/4$	$\pi/4$	π	0.9973±0.0002	0.9982±0.0002
HV	$\pi/2$	$\pi/2$	0	0.9992±0.0001	0.9992±0.0001

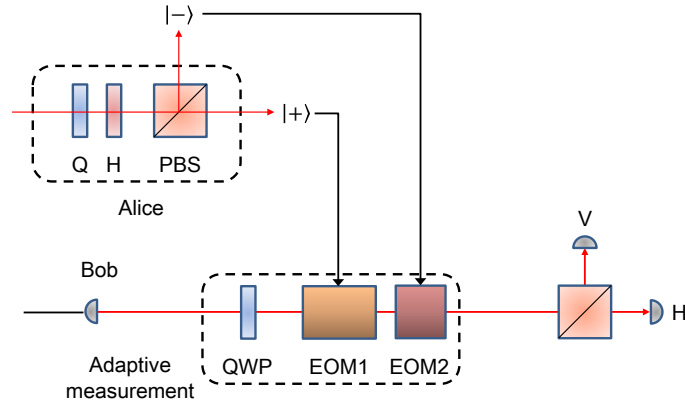
Determine the target state. For our target state defined in Eq. (25), θ and ϕ are two parameters to be set experimentally. For each k , we first calculate the ratio of HV component to VH component, i.e., $(\sin \theta / \cos \theta)^2$, in the target state. Based on this ratio, we rotate the angles of QWP1 and HWP1 of pump light to generate this target state. Then, the density matrix ρ of the target state can be obtained by means of the maximum likelihood estimations. The overlap between $|\psi\rangle$ and ρ is used as our objective function. A global search algorithm is used to minimize the objective function $1 - \langle \psi | \rho | \psi \rangle$ with θ and ϕ as two free parameters in $|\psi\rangle$. Finally, we obtain the values of these two parameters with our optimization program⁴.

The projective measurements. The nonadaptive strategy requires four projective measurements. From the expression of the four projectors (Eq. (29-35)), we can see that P_0 is the standard σ_z projection while P_i ($i = 1, 2, 3$) are three general projectors that are realized by rotating the angles of wave plates in the state analyser (see Fig. 2 in main text). The function of P_i projectors is to transform the $|\tilde{u}_i\rangle$ and $|\tilde{v}_i\rangle$ states to the $|H\rangle$ state with combinations of QWP and HWP. Therefore, we treat the angles of QWP and HWP as two quantities to realize the transformation utilizing Jones matrix method. By solving the equations, we find the angles of wave plates that realizes the four projective measurements.

For the adaptive strategy, three measurements \tilde{T}_0 , \tilde{T}_1 and \tilde{T}_2 are required. From Eq. (37-43), we can see that \tilde{T}_0 is the standard σ_z projection. The \tilde{T}_1 and \tilde{T}_2 measurements requires classical communication to transmit the results of Alice's measurements to Bob. Then Bob applies the corresponding measurements using the electro-optic modulators (EOMs) according to Alice's results. For \tilde{T}_1 , Alice implements the $\{|+\rangle, |-\rangle\}$ orthogonal measurements while Bob's two measurements $|\tilde{v}_+\rangle$ and $|\tilde{v}_-\rangle$ are nonorthogonal. For \tilde{T}_2 , Alice's measurements $\{|R\rangle, |L\rangle\}$ are orthogonal whereas Bob need to apply the nonorthogonal measurements $|\tilde{w}_+\rangle$ and $|\tilde{w}_-\rangle$ accordingly. In the following, we describe how to realize these adaptive measurements by means of local operations and classical communication (LOCC) in real time.

In order to implement the $\{|\tilde{v}_+\rangle, |\tilde{v}_-\rangle\}$ and $\{|\tilde{w}_+\rangle, |\tilde{w}_-\rangle\}$ measurements at Bob's site according to Alice's measurement outcomes, we use two EOMs, as shown in Supplementary Figure 1. The $|\tilde{v}_+\rangle$ and $|\tilde{w}_+\rangle$ polarized states are

rotated to H polarization with EOM1, which finally exit from the transmission port of polarized beam splitter (PBS, the wave plates before PBS are rotated to HV bases). Correspondingly, the $|\tilde{v}_-\rangle$ and $|\tilde{w}_-\rangle$ are transformed to the V polarization with EOM2 and exit from the reflection port of PBS. We use the output of $|+\rangle/|R\rangle$ to trigger the EOM1 and the output of $|-\rangle/|L\rangle$ to trigger the EOM2, respectively. This design guarantees that only one EOM takes effect and the other executes the identity operation for each of the generated state. In Supplementary Table 2, we list the operations realized with these two EOMs. We can see that the adaptive measurements are genuinely realized with our setup.



Supplementary Figure 1 The adaptive measurements implemented with electro-optic modulator (EOM). Here we take \tilde{T}_1 measurement as an illustration. The output signal of $|+\rangle$ is used to trigger EOM1 to execute the $|\tilde{v}_+\rangle$ measurement, while the output signal of $|-\rangle$ is used to trigger EOM2 to execute the $|\tilde{v}_-\rangle$ measurement. Only one EOM is triggered at a time and the other EOM is an identity operation, which guarantees the adaptive measurements are realized in real time. A QWP before the two EOMs is used to compensate the extra phase from \tilde{T}_1 to \tilde{T}_2 measurement.

There are two key ingredients for our adaptive measurement that distinguish it from the nonadaptive measurement. First, Alice produces binary outcomes for a given basis. In each run, only one of these two outcomes will be obtained. Bob's measurements have to be adaptive according to Alice's measurement results. Second, it doesn't require fast changes among the \tilde{T}_0 , \tilde{T}_1 and \tilde{T}_2 measurements. This can be seen from the fact that $\{|\tilde{w}_+\rangle, |\tilde{w}_-\rangle\}$ have an extra $\pi/2$ phase compared with the $\{|\tilde{v}_+\rangle, |\tilde{v}_-\rangle\}$ bases (see Eqs. (42,43)). We add a QWP (see Supplementary Figure 1) before the two EOMs to compensate this extra phase. We calibrate the optical axis of these two EOMs and fix them. If we want to perform from \tilde{T}_1 to \tilde{T}_2 measurement or vice versa, we add or remove this QWP. For \tilde{T}_0 measurement, we turn off the drivers of these two EOMs and remove the QWP. In the single-photon experiment, we can optimize the modulation contrast of these two EOMs with the coincidence ratio of $CC_{+\tilde{v}_+}/CC_{+\tilde{v}_\perp}$ and $CC_{-\tilde{v}_-}/CC_{-\tilde{v}_\perp}$ as our optimization goals (see Supplementary Table 2).

Supplementary Note 3. APPLYING THE VERIFICATION STRATEGY TO TASK B

In this section, we explain in detail how we use the verification strategy proposed in Supplementary Note 1 to execute **Task B**. Generally speaking, **Task B** is to distinguish whether the quantum device outputs states ϵ -far away from

Supplementary Table 2 Adaptive measurements $\{\tilde{T}_0, \tilde{T}_1, \tilde{T}_2\}$ realized with two EOMs.

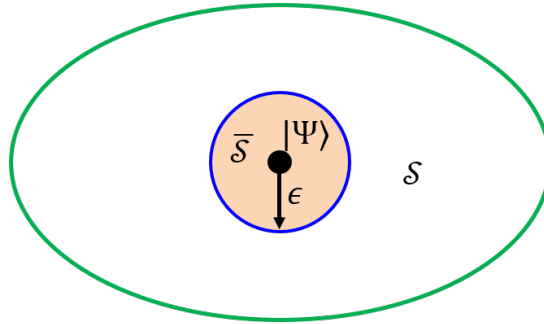
Setting	Alice	Bob's operations		Output	Modulation contrast*	Success probability
\tilde{T}_0	H	I (EOM1)	I (EOM2)	—	CC_{HV}/CC_{HH}	$\frac{CC_{HV}+CC_{VH}}{CC_{HV}+CC_{HH}+CC_{VV}+CC_{VH}}$
	V	I (EOM1)	I (EOM2)	—	CC_{VH}/CC_{VV}	
\tilde{T}_1	$+$	\tilde{v}_+ (EOM1)	I (EOM2)	$\tilde{v}_+ \rightarrow H$	$CC_{+\tilde{v}_+}/CC_{+\tilde{v}_+^\perp}$	$\frac{CC_{+\tilde{v}_+}+CC_{-\tilde{v}_-}}{CC_{+\tilde{v}_+}+CC_{+\tilde{v}_-}+CC_{-\tilde{v}_+}+CC_{-\tilde{v}_-}}$
	$-$	I (EOM1)	\tilde{v}_- (EOM2)	$\tilde{v}_- \rightarrow V$	$CC_{-\tilde{v}_-}/CC_{-\tilde{v}_-^\perp}$	
\tilde{T}_2	R	\tilde{w}_+ (EOM1)	I (EOM2)	$\tilde{w}_+ \rightarrow H$	$CC_{R\tilde{w}_+}/CC_{R\tilde{w}_+^\perp}$	$\frac{CC_{R\tilde{w}_+}+CC_{L\tilde{w}_-}}{CC_{R\tilde{w}_+}+CC_{R\tilde{w}_-}+CC_{L\tilde{w}_+}+CC_{L\tilde{w}_-}}$
	L	I (EOM1)	\tilde{w}_- (EOM2)	$\tilde{w}_- \rightarrow V$	$CC_{L\tilde{w}_-}/CC_{L\tilde{w}_-^\perp}$	

* $\tilde{v}_+^\perp/\tilde{w}_+^\perp$ and $\tilde{v}_-^\perp/\tilde{w}_-^\perp$ are the orthogonal states to \tilde{v}_+/\tilde{w}_+ and \tilde{v}_-/\tilde{w}_- , respectively.

the target state $|\Psi\rangle$ or not. Let \mathcal{S} be the set of states that are at least ϵ -far always from $|\Psi\rangle$, i.e.,

$$\mathcal{S} := \{\sigma_i : \langle \Psi | \sigma_i | \Psi \rangle \leq 1 - \epsilon\}, \quad (53)$$

and $\bar{\mathcal{S}}$ to be the complement of \mathcal{S} , which is the set of states that are ϵ -close to $|\Psi\rangle$. See Supplementary Figure 2 for illustration.



Supplementary Figure 2 \mathcal{S} is the set of states that are at least ϵ -far always from $|\Psi\rangle$, that is, states that are out of the brown circle. The states that are on the circle (the blue circle, $\langle \Psi | \sigma | \Psi \rangle = 1 - \epsilon$) are the most difficult to be distinguished from $|\Psi\rangle$, compared to states in \mathcal{S} .

Before going to the details, we compare briefly the differences between **Task A** and **Task B**.

1. **Task A**^{1,2} considers the problem: Performing tests sequentially, how many tests are required before we identify a σ_i that does not pass the test? Once we find a σ_i not passing the test, we conclude that the device is bad. Each test is a Bernoulli trial with probability Δ_ϵ determined by the chosen verification strategy. The expected number of tests required is given by $1/\Delta_\epsilon$. It should be stressed that this expectation is achieved with the assumption that all generated states are ϵ -far from $|\Psi\rangle$. Once the generated states are much further from $|\Psi\rangle$ by ϵ (**Case 2**), then the observed number of tests will be less than $1/\Delta_\epsilon$.
2. **Task B**⁵ considers the problem: Performing N tests, how many states σ_i can pass these tests on average? If all generated states are *exactly* ϵ -far from $|\Psi\rangle$, then the expected number of states passing the test is $N\mu$, where μ is the expected passing probability of each generated state, determined by the chosen verification strategy. If

all generated states are much far from $|\Psi\rangle$ by ϵ (**Case 2**), then the expected number of states passing the test is less than $N\mu$. If all generated states are much close to $|\Psi\rangle$ by ϵ (**Case 1**), then the expected number of states passing the test is larger than $N\mu$.

A. Applying the nonadaptive strategy to Task B

Here we illustrate how to use the nonadaptive verification strategy Ω_{opt} proposed in [Supplementary Note 1 A](#) to execute **Task B**. First of all, the following two lemmas are essential, which state that for arbitrary state belonging to \mathcal{S} ($\bar{\mathcal{S}}$), its probability of passing the test Ω_{opt} is upper (lower) bounded.

Lemma 2. *For arbitrary state $\sigma \in \mathcal{S}$, it can pass Ω_{opt} with probability no larger than $1 - [1 - \lambda_2(\Omega_{\text{opt}})]\epsilon$, where $\lambda_2(\Omega_{\text{opt}})$ is the second largest eigenvalue of Ω_{opt} given in Eq. (8). The upper bound is achieved by states in \mathcal{S} that are exactly ϵ -far from $|\Psi\rangle$.*

Intuitively, the further a state $\sigma \in \mathcal{S}$ is from $|\Psi\rangle$, the smaller the probability it passes the test Ω_{opt} . Lemma 2 justifies this intuition and shows quantitatively that the passing probability for states in \mathcal{S} cannot be larger than $1 - [1 - \lambda_2(\Omega_{\text{opt}})]\epsilon$. However, we remark that it is possible that for some states in \mathcal{S} the passing probability is small.

Proof. From the spectral decomposition Eq. (10) of Ω_{opt} and the fact that the off-diagonal parts of σ do not affect the trace $\text{Tr}[\Omega_{\text{opt}}\sigma]$, we can assume without loss of generality that σ has the form

$$\sigma = p_1|\Psi\rangle\langle\Psi| + p_2|\Psi^\perp\rangle\langle\Psi^\perp| + p_3|HV\rangle\langle HV| + p_4|VH\rangle\langle VH|, \quad \sum_{i=1}^4 p_i = 1, \quad p_1 \leq 1 - \epsilon, \quad (54)$$

where the last constraint $p_1 \leq 1 - \epsilon$ follows from the precondition that $\sigma \in \mathcal{S}$. Then

$$\begin{aligned} \text{Tr}[\Omega_{\text{opt}}\sigma] &= p_1 + \sum_{i=2}^4 \lambda_i p_i \\ &\leq p_1 + (1 - p_1)\lambda_2 \\ &\leq (1 - \epsilon)(1 - \lambda_2) + \lambda_2 \\ &= 1 - (1 - \lambda_2)\epsilon, \end{aligned} \quad (55)$$

where λ_i is the i -th eigenvalue of Ω_{opt} , the first inequality follows from $\lambda_2 \geq \lambda_3 \geq \lambda_4$ and the second inequality follows from $p_1 \leq 1 - \epsilon$. \square

Lemma 3. *For arbitrary state $\sigma \in \bar{\mathcal{S}}$, it can pass the nonadaptive strategy Ω_{opt} with probability no smaller than $1 - [1 - \lambda_2(\Omega_{\text{opt}})]\epsilon$. The lower bound is achieved by states in $\bar{\mathcal{S}}$ that are exactly ϵ -far from $|\Psi\rangle$.*

Proof. Following the proof for Lemma 2 and considering the spectral decomposition Eq. (10) of Ω_{opt} , we can assume without loss of generality that σ has the form

$$\sigma = p_1|\Psi\rangle\langle\Psi| + p_2|\Psi^\perp\rangle\langle\Psi^\perp| + p_3|VH\rangle\langle VH| + p_4|HV\rangle\langle HV|, \quad \sum_{i=1}^4 p_i = 1, \quad p_1 \geq 1 - \epsilon, \quad (56)$$

where the last constraint $p_1 \geq 1 - \epsilon$ follows from the precondition that $\sigma \in \overline{\mathcal{S}}$. Then

$$\begin{aligned}
\text{Tr} [\Omega_{\text{opt}} \sigma] &= p_1 + \lambda_2(\Omega_{\text{opt}}) \sum_{i=2}^4 p_i \\
&= p_1 + \lambda_2(\Omega_{\text{opt}})(1 - p_1) \\
&\geq (1 - \epsilon)(1 - \lambda_2(\Omega_{\text{opt}})) + \lambda_2(\Omega_{\text{opt}}) \\
&= 1 - (1 - \lambda_2(\Omega_{\text{opt}}))\epsilon,
\end{aligned} \tag{57}$$

where the first equality follows from the spectral decomposition of Eq. (10) and the inequality follows from $p_1 \geq 1 - \epsilon$. \square

Task B is to distinguish among the following *two* cases for a given quantum device \mathcal{D} :

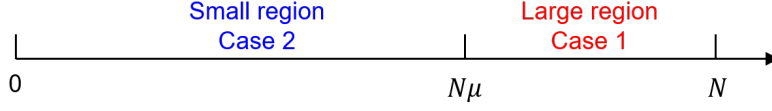
Case 1: $\forall i, \sigma_i \in \overline{\mathcal{S}}$. That is, the device always generate states that are sufficient close to the target state $|\Psi\rangle$. If it is the case, we regard the device as “good”.

Case 2: $\forall i, \sigma_i \in \mathcal{S}$. That is, the device always generate states that are sufficient far from the target state $|\Psi\rangle$. If it is the case, we regard the device as “bad”.

To execute **Task B**, we perform N tests on the outputs of the device with Ω_{opt} and record the number of tests that pass the test as m_{pass} . What conclusion can we obtain from the relation between m_{pass} and N ? From Lemma 2, we know that if the device is bad (belonging to **Case 2**), m_{pass} cannot be too large, since the passing probability of each generated state is upper bounded. Conversely, Lemma 3 guarantees that if the device is good (belonging to **Case 1**), m_{pass} cannot be too small, since the passing probability of each generated state is lower bounded. Let’s then justify this intuition rigorously. We define the binary random variable X_i to represent the event that whether state σ_i passes the test or not. If it passes, we set $X_i = 1$; If it fails to pass the test, we set $X_i = 0$. After N tests, we obtain a sequence of independent distribution random variables $\{X_i\}_{i=1}^N$. Then $m_{\text{pass}} = \sum_{i=1}^N X_i$. Now let’s analyze the expectation of each X_i . Let $\mu := 1 - [1 - \lambda_2(\Omega_{\text{opt}})]\epsilon$. If the device were ‘good’ (it belongs to **Case 1**), then Lemma 3 implies that the expectation of X_i , denoted as $\mathbb{E}(X_i)$, shall satisfy $\mathbb{E}(X_i) \geq \mu$. The independent assumption together with the law of large numbers guarantee $m_{\text{pass}} \geq N\mu$, when N is sufficiently large. On the other hand, if the device were ‘bad’ (it belongs to **Case 2**), then Lemma 2 asserts that the expectation of X_i shall satisfy $\mathbb{E}(X_i) \leq \mu$. Again, the independent assumption together with the law of large numbers guarantee $m_{\text{pass}} \leq N\mu$, when N is sufficiently large. That is to say, we consider two regions regarding the value of m_{pass} : the region that $m_{\text{pass}} \leq N\mu$ and the region that $m_{\text{pass}} \geq N\mu$. We refer to Supplementary Figure 3 for illustration.

Large Region: $m_{\text{pass}} \geq N\mu$. In this region, the device belongs to **Case 1** with high probability, as only in this case m_{pass} can be large. Following the analysis methods in refs.⁵⁻⁸, we use the Chernoff bound to upper bound the probability that the device belongs to **Case 2** as

$$\delta \equiv e^{-N D\left(\frac{m_{\text{pass}}}{N} \parallel \mu\right)}, \tag{58}$$



Supplementary Figure 3 The number of copies m_{pass} that pass the nonadaptive strategy Ω_{opt} determines the quality of the device. If $m_{\text{pass}} \leq N\mu$, the device is very likely to be **Case 2 (Small Region)**. Conversely, the device is very likely to be **Case 1 (Large Region)** if $m_{\text{pass}} \geq N\mu$.

where $D(x||y) := x \log_2 \frac{x}{y} + (1-x) \log_2 \frac{1-x}{1-y}$ the Kullback-Leibler divergence. That is to say, if the device *did* belong to **Case 2**, the probability that m_{pass} is larger than $N\mu$ decays exponentially as m_{pass} becomes larger. In this case, we reach a conclusion:

*The device belongs to **Case 2** with probability at most δ .*

Equivalently, we conclude that

*The device belongs to **Case 1** with probability at least $1 - \delta$.*

Small Region: $m_{\text{pass}} \leq N\mu$. The analysis for this region is almost the same as that of the large region. In this region, the device belongs to **Case 2** with high probability, as only in this case m_{pass} can be smaller than $N\mu$. Following the analysis methods in refs.⁵⁻⁸, we use the Chernoff bound to upper bound the probability that the device belongs to **Case 1** as

$$\delta \equiv e^{-N D(\frac{m_{\text{pass}}}{N} || \mu)}. \quad (59)$$

That is to say, if the device *did* belong to **Case 1**, the probability that m_{pass} is less than $N\mu$ decays exponentially as m_{pass} becomes smaller. In this case, we reach a conclusion:

*The device belongs to **Case 1** with probability at most δ .*

Equivalently, we conclude that

*The device belongs to **Case 2** with probability at least $1 - \delta$.*

B. Applying the adaptive strategy to Task B

The way that we use the adaptive verification strategy $\Omega_{\text{opt}}^{\rightarrow}$ proposed in [Supplementary Note 1 B](#) to execute **Task B** is similar to that discussed in the previous section. The following two lemmas are required, which state that for arbitrary state belonging to \mathcal{S} ($\bar{\mathcal{S}}$), its probability of passing the test $\Omega_{\text{opt}}^{\rightarrow}$ is upper (lower) bounded.

Lemma 4. *For arbitrary state $\sigma \in \mathcal{S}$, it can pass $\Omega_{\text{opt}}^{\rightarrow}$ with probability no larger than $1 - [1 - \lambda_2(\Omega_{\text{opt}}^{\rightarrow})]\epsilon$, where $\lambda_2(\Omega_{\text{opt}}^{\rightarrow})$ is the second largest eigenvalue of $\Omega_{\text{opt}}^{\rightarrow}$ given in Eq. (18). The upper bound is achieved by states in \mathcal{S} that are exactly ϵ -far from $|\Psi\rangle$.*

The proof of Lemma 4 is the same as that of Lemma 2, so we omit the details.

Lemma 5. *For arbitrary state $\sigma \in \overline{\mathcal{S}}$, it can pass the adaptive strategy $\Omega_{\text{opt}}^{\rightarrow}$ with probability no smaller than $1 - [1 - \lambda_4(\Omega_{\text{opt}}^{\rightarrow})]\epsilon$, where $\lambda_4(\Omega_{\text{opt}}^{\rightarrow}) = \sin^2 \theta / (1 + \cos^2 \theta)$ is the fourth (also the smallest) eigenvalue of $\Omega_{\text{opt}}^{\rightarrow}$. The lower bound is achieved by states in $\overline{\mathcal{S}}$ that are exactly ϵ -far from $|\Psi\rangle$.*

Proof. Following the proof for Lemma 3 and considering the spectral decomposition Eq. (20) of $\Omega_{\text{opt}}^{\rightarrow}$, we can assume without loss of generality that σ has the form

$$\sigma = p_1 |\Psi\rangle\langle\Psi| + p_2 |\Psi^\perp\rangle\langle\Psi^\perp| + p_3 |VH\rangle + p_4 |HV\rangle, \quad \sum_{i=1}^4 p_i = 1, \quad p_1 \geq 1 - \epsilon, \quad (60)$$

where the last constraint $p_1 \geq 1 - \epsilon$ follows from the precondition that $\sigma \in \overline{\mathcal{S}}$. Then

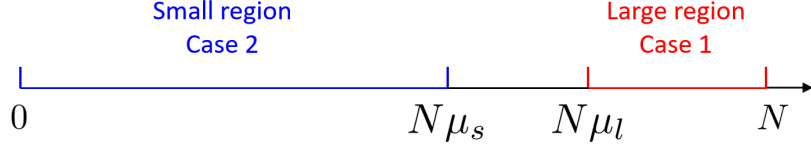
$$\begin{aligned} \text{Tr} [\Omega_{\text{opt}}^{\rightarrow} \sigma] &= p_1 + \sum_{i=2}^4 \lambda_i(\Omega_{\text{opt}}^{\rightarrow}) p_i \\ &\geq p_1 + \lambda_4(\Omega_{\text{opt}}^{\rightarrow}) \sum_{i=2}^4 p_i \\ &= p_1 + \lambda_4(\Omega_{\text{opt}}^{\rightarrow}) (1 - p_1) \\ &\geq (1 - \epsilon)(1 - \lambda_4(\Omega_{\text{opt}}^{\rightarrow})) + \lambda_4(\Omega_{\text{opt}}^{\rightarrow}) \\ &= 1 - (1 - \lambda_4(\Omega_{\text{opt}}^{\rightarrow}))\epsilon, \end{aligned} \quad (61)$$

where the first inequality follows from the fact that $\lambda_4(\Omega_{\text{opt}}^{\rightarrow})$ is the smallest eigenvalue of $\Omega_{\text{opt}}^{\rightarrow}$ and the second inequality follows from $p_1 \geq 1 - \epsilon$. \square

To execute **Task B**, we perform N tests on the outputs of the device with $\Omega_{\text{opt}}^{\rightarrow}$ and record the number of tests that pass the test as m_{pass} . Define the binary random variable X_i to present the event that whether state σ_i passes the test or not. If it passes, we set $X_i = 1$; If it fails to pass the test, we set $X_i = 0$. After N tests, we obtain a sequence of independent random variables $\{X_i\}_{i=1}^N$. Then $m_{\text{pass}} = \sum_{i=1}^N X_i$. We analyze the expectation of each X_i . Let $\mu_l := 1 - [1 - \lambda_2(\Omega_{\text{opt}}^{\rightarrow})]\epsilon$ and $\mu_s := 1 - [1 - \lambda_4(\Omega_{\text{opt}}^{\rightarrow})]\epsilon$. If the device were ‘good’ (it belongs to **Case 1**), then Lemma 5 implies that $\mathbb{E}(X_i) \geq \mu_s$. The independent assumption together with the law of large numbers guarantee $m_{\text{pass}} \geq N\mu_s$, when N is sufficiently large. That is to say, if in practical it turns out that $m_{\text{pass}} \leq N\mu_s$, then we are pretty sure the device is bad. On the other hand, if the device were ‘bad’ (it belongs to **Case 2**), then Lemma 4 asserts that $\mathbb{E}(X_i) \leq \mu_l$. Again, the independent assumption together with the law of large numbers guarantee $m_{\text{pass}} \leq N\mu_l$, when N is sufficiently large. That is, if in practical it turns out that $m_{\text{pass}} \geq N\mu_l$, then we are pretty sure the device is good. Thus, we shall consider two regions regarding the value of m_{pass} : the region that $m_{\text{pass}} \leq N\mu_s$ and the region that $m_{\text{pass}} \geq N\mu_l$. We refer to Supplementary Figure 4 for illustration.

Large Region: $m_{\text{pass}} \geq N\mu_l$. In this region, the device belongs to **Case 1** with high probability. Following the analysis methods in refs.⁵⁻⁸, we use the Chernoff bound to upper bound the probability that the device belongs to **Case 2** as

$$\delta_l \equiv e^{-N D\left(\frac{m_{\text{pass}}}{N} \parallel \mu_l\right)}. \quad (62)$$



Supplementary Figure 4 The number of copies m_{pass} that pass the adaptive strategy $\Omega_{\text{opt}}^{\rightarrow}$ determines the quality of the device. If $m_{\text{pass}} \leq N\mu_s$, the device belongs very likely to **Case 2 (Small Region)**. Conversely, the device belongs with high probability to **Case 1 (Large Region)** if $m_{\text{pass}} \geq N\mu_l$.

That is to say, if the device *did* belong to **Case 2**, the probability that m_{pass} is larger than $N\mu$ decays exponentially when m_{pass} becomes large. In this case, we reach a conclusion:

*The device belongs to **Case 2** with probability at most δ_l .*

Equivalently, we conclude that

*The device belongs to **Case 1** with probability at least $1 - \delta_l$.*

Small Region: $m_{\text{pass}} \leq N\mu_s$. The analysis for this region is almost the same as that of the large region. In this region, the device belongs to **Case 2** with high probability, as only in this case m_{pass} can be smaller than $N\mu_s$. Following the analysis methods in refs.⁵⁻⁸, we use the Chernoff bound to upper bound the probability that the device belongs to **Case 1** as

$$\delta_s \equiv e^{-N D\left(\frac{m_{\text{pass}}}{N} \parallel \mu_s\right)}, \quad (63)$$

That is to say, if the device *did* belong to **Case 1**, the probability that m_{pass} is less than $N\mu$ decays exponentially as m_{pass} becomes smaller. In this case, we reach a conclusion:

*The device belongs to **Case 1** with probability at most δ_s .*

Equivalently, we conclude that

*The device belongs to **Case 2** with probability at least $1 - \delta_s$.*

Supplementary Note 4. THE EXPERIMENTAL RESULTS FOR THE THREE TARGET STATES

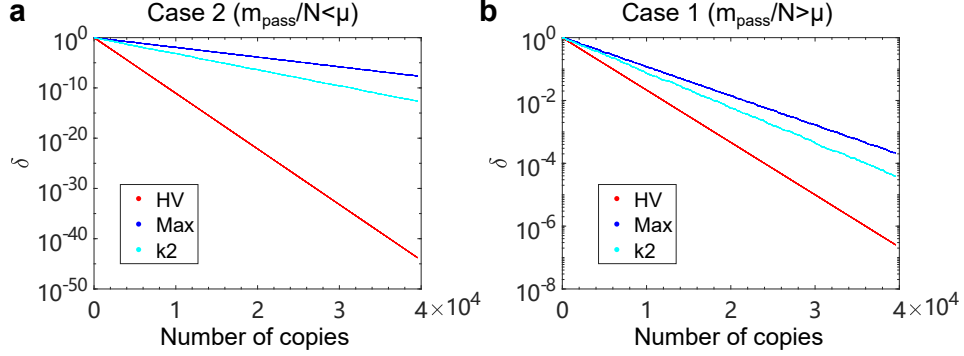
In this section, we give the results for three target states, i.e., k2, Max and HV (see Supplementary Table 1). Note that the failing probability for each measurement is different for the three states¹

$$\text{k2} : \Delta_{\epsilon} = \frac{\epsilon}{2 + \sin \theta \cos \theta} \quad (64a)$$

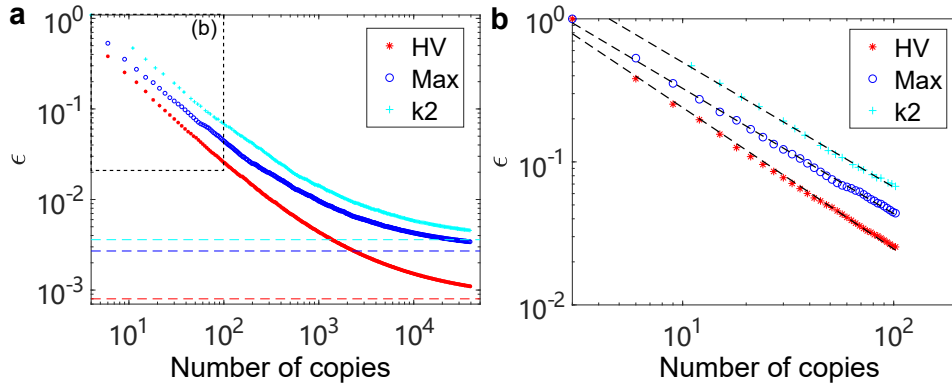
$$\text{Max} : \Delta_{\epsilon} = \frac{2\epsilon}{3} \quad (64b)$$

$$\text{HV} : \Delta_{\epsilon} = \epsilon \quad (64c)$$

Here we discuss the results of the nonadaptive strategy. In Eq. (64), ϵ can be replaced with $1 - F$, where F is the fidelity for corresponding states. From the experimental data, the stable passing probability m_{pass}/N can be obtained, which are 0.9986 ± 0.0002 , 0.9982 ± 0.0002 and 0.9992 ± 0.0001 , respectively. With $\mu = 1 - \Delta_\epsilon = m_{\text{pass}}/N$, we have an estimation for the fidelities of these three states, which are $F_{k2} = 0.9964 \pm 0.0002$, $F_{\text{Max}} = 0.9973 \pm 0.0002$ and $F_{\text{HV}} = 0.9992 \pm 0.0001$. The variation of δ versus N for the three target states is shown in Supplementary Figure 5 in the log scale. To make the comparison fairly, we take $\eta := |\mu - m_{\text{pass}}/N|$ to be same for the three states. In this condition, the slope of decline (i.e., g in $\log \delta \propto g \cdot N$) is $g_{\text{HV}} > g_{k2} > g_{\text{Max}}$, which indicates that the state with a larger passing probability will have a faster decline.



Supplementary Figure 5 Experimental results on the variation of δ versus the number of copies for the three target states. Here the difference $\eta := |\mu - m_{\text{pass}}/N|$ is set the same for the three states. The small region (a) decrease faster than the large region (b), which indicates it is easier to verify **Case 2** than **Case 1**. The state with a larger passing probability will have a faster slope of decline. Note that the experimental data symbols shown in the figure looks like lines due to the dense data points.



Supplementary Figure 6 Experimental results on the variation of ϵ versus the number of copies for the three target states. The ϵ will finally approach the asymptotic line of the infidelities 0.0036 ± 0.0002 , 0.0027 ± 0.0002 and 0.0008 ± 0.0001 for these three states. **b** is the linear region of the enlarged dashed box in **a**. We fit the linear region (dashed black line) and obtain slopes of -0.88 ± 0.03 , -0.87 ± 0.10 and -0.99 ± 0.09 for k2, Max and HV states, respectively.

In Supplementary Figure 6, we present the results of ϵ versus N . We can see that ϵ first decreases linearly with N and then approaches a asymptote in the log-log scale. The asymptotic values for these three states are the infidelities

calculated from Eq. (64), which are 0.0036 ± 0.0002 , 0.0027 ± 0.0002 and 0.0008 ± 0.0001 , respectively. To see the scaling of ϵ versus N , the region for the number of copies from 1-100 is enlarged and shown in Supplementary Figure 6b. The linear scaling region is fitted with slopes of -0.88 ± 0.03 , -0.87 ± 0.10 and -0.99 ± 0.09 , respectively. The error bars are obtained by fitting different groups of ϵ versus N when considering the errors of ϵ (shown in Fig. 5 of the main text).

Supplementary Note 5. EXPLANATIONS FOR THE RESULTS IN TASK A

In this section, we explain on the difference of experimental and theoretical improvements for the number of measurements required in **Task A** of main text. Consider a general state ρ produced in the experiment that is exactly ϵ -far from $|\Psi\rangle$, which can be diagonalized in the bases $\{|\Psi\rangle, |\Psi^\perp\rangle, |HV\rangle, |VH\rangle\}$ as:

$$\rho = (1 - \epsilon)|\Psi\rangle\langle\Psi| + p_2|\Psi^\perp\rangle\langle\Psi^\perp| + p_3|HV\rangle\langle HV| + p_4|VH\rangle\langle VH|, \quad (65)$$

where the normalization condition requires $p_2 + p_3 + p_4 = \epsilon$. Given the spectral decomposition of Ω_{opt} in Eq. (10), the passing probability of ρ that passes the nonadaptive strategy Ω_{opt} can be expressed as

$$\begin{aligned} \text{Tr}[\Omega_{\text{opt}}\rho] &= 1 - \epsilon + \lambda_2(\Omega_{\text{opt}})(p_2 + p_3 + p_4) \\ &= 1 - [1 - \lambda_2(\Omega_{\text{opt}})]\epsilon \\ &= 1 - \frac{1}{2 + \sin\theta \cos\theta} \epsilon \\ &\equiv 1 - \Delta_\epsilon. \end{aligned} \quad (66)$$

From Eq. (66) we can see that the passing probability of nonadaptive strategy is independent on p_2 , p_3 and p_4 .

Likewise, the passing probability of the adaptive strategy $\Omega_{\text{opt}}^\rightarrow$ can be expressed as,

$$\begin{aligned} \text{Tr}[\Omega_{\text{opt}}^\rightarrow\rho] &= 1 - \epsilon + \lambda_2(\Omega_{\text{opt}}^\rightarrow)(p_2 + p_3) + \lambda_4(\Omega_{\text{opt}}^\rightarrow)p_4 \\ &= 1 - \epsilon + \lambda_2(\Omega_{\text{opt}}^\rightarrow)(p_2 + p_3 + p_4) - (\lambda_2(\Omega_{\text{opt}}^\rightarrow) - \lambda_4(\Omega_{\text{opt}}^\rightarrow))p_4 \\ &= 1 - (1 - \lambda_2(\Omega_{\text{opt}}^\rightarrow))\epsilon - (\lambda_2(\Omega_{\text{opt}}^\rightarrow) - \lambda_4(\Omega_{\text{opt}}^\rightarrow))p_4 \\ &= 1 - \frac{1}{1 + \cos^2\theta} \epsilon - \frac{\cos^2\theta - \sin^2\theta}{1 + \cos^2\theta} p_4 \\ &\equiv 1 - \Delta_\epsilon^\rightarrow. \end{aligned} \quad (67)$$

We can see that the passing probability of adaptive is not only dependent on the ϵ , but also dependent on p_4 . Note that the number of measurements required to obtain a $1 - \delta$ confidence and infidelity ϵ is given by $n \propto \frac{1}{\Delta_\epsilon} \ln \frac{1}{\delta}$. Therefore, the improvement of adaptive relative to nonadaptive is,

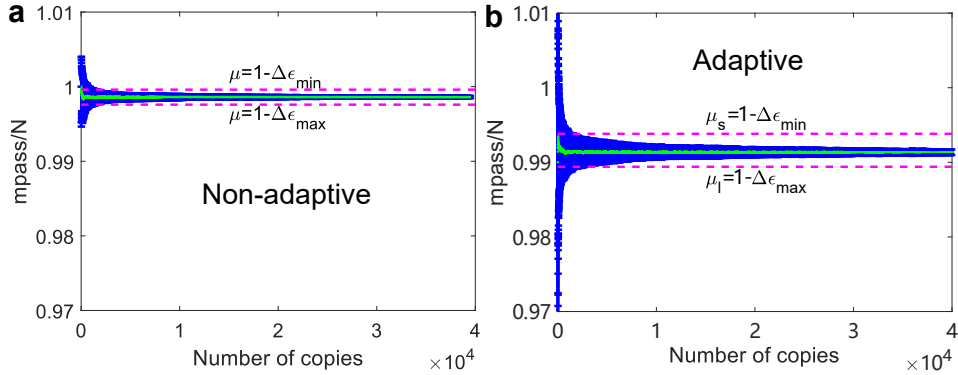
$$\frac{n^{\text{Non}}}{n^{\text{Adp}}} \propto \frac{\Delta_\epsilon^\rightarrow}{\Delta_\epsilon}. \quad (68)$$

From Eqs. (66) and (67), we can see that the ratio of the coefficient of ϵ , i.e., $(2 + \sin\theta \cos\theta):(1 + \cos^2\theta)$, is just the theoretical prediction, which is about 1.6 times for the $k2$ state. The remaining term is dependent on p_4 in Eq. (67). On the other hand, the experimental limited fidelity of the EOMs' modulation will result in a lower passing probability

of the adaptive measurement. This also leads to a larger $\Delta_\epsilon^\rightarrow$ in Eq. (67), which improves the ratio. Based on our experimental data, we give a quantitative estimation. The failing probability of nonadaptive is about $\Delta_\epsilon \sim 0.0014$ (see Supplementary Table 1). If the passing probability of adaptive is decreased by 0.007, the number of copies will have a $0.007/0.0014 \sim 5$ times reduction due to such a small denominator of Δ_ϵ . This leads to the overall about six times fewer number of copies cost by the adaptive strategy compared with the nonadaptive strategy.

Supplementary Note 6. COMPARISON OF NONADAPTIVE AND ADAPTIVE IN TASK B

In Supplementary Figure 7, we give the variation of experimental passing probability m_{pass}/N versus the number of copies. For clearness, we also plot the expected passing probability $\mu = 1 - \Delta_\epsilon$ which is chosen by the verifier. The ϵ_{min} is adopted for **Case 2** and the ϵ_{max} is adopted for **Case 1**. With enough number of copies of quantum states, the passing probability m_{pass}/N will reach a stable value. It can be seen that the experimental passing probability is smaller than the expectation for **Case 2** while it is larger for **Case 1**. The stable passing probability of adaptive 0.9914 ± 0.0005 is smaller than the nonadaptive strategy 0.9986 ± 0.0002 due to their different infidelities.

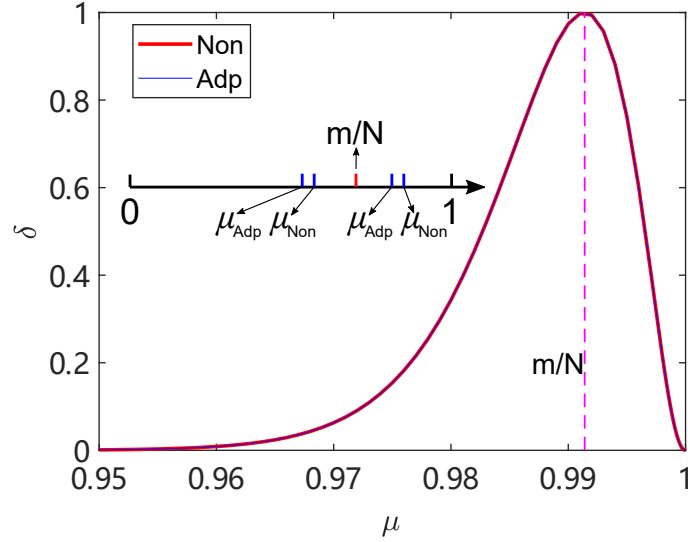


Supplementary Figure 7 Experimental results on the variation of passing probability m_{pass}/N versus number of copies for $\epsilon = \epsilon_{\text{min}}$ and $\epsilon = \epsilon_{\text{max}}$. **a** are for the nonadaptive strategy, while **b** are for the adaptive strategy. The dashed magenta line is the corresponding expected passing probability $\mu = 1 - \Delta_{\epsilon_{\text{min}}}/\mu = 1 - \Delta_{\epsilon_{\text{max}}}$ chosen by the verifier for the nonadaptive strategy. For adaptive strategy, the ϵ_{min} (ϵ_{max}) is chosen so that $m_{\text{pass}}/N < \mu_s$ ($m_{\text{pass}}/N > \mu_l$). The experimental passing probability m_{pass}/N reaches a stable value after about 1000 number of copies. The adaptive m_{pass}/N is smaller than the nonadaptive. The blue is the experimental error bar, which is obtained by 100 rounds for each copy.

In the main text, we see that the scaling behaviour of parameters δ and ϵ versus number of copies N is different for nonadaptive and adaptive strategies in **Task B**. Here, we give some analyses to explain.

For the variation of δ versus N , the speed of descent is determined by the difference between experimental passing probability m_{pass}/N and expected passing probability $\mu = 1 - \Delta_\epsilon$. Because the nonadaptive and adaptive strategy have different m_{pass}/N and μ , the behaviour of δ versus N is also different. To have a comprehensive understanding, we consider two situations. First, we assume they have the same m_{pass}/N and the same ϵ . The expected passing probabilities are $\mu_{\text{Non}} = 1 - \epsilon/(2 + \sin\theta \cos\theta)$ and $\mu_{\text{Adp}} = 1 - \epsilon/(2 - \sin^2\theta)$ for nonadaptive and adaptive strategies, respectively. We can see that μ_{Non} is larger than μ_{Adp} under the same ϵ . In Supplementary Figure 8, we plot

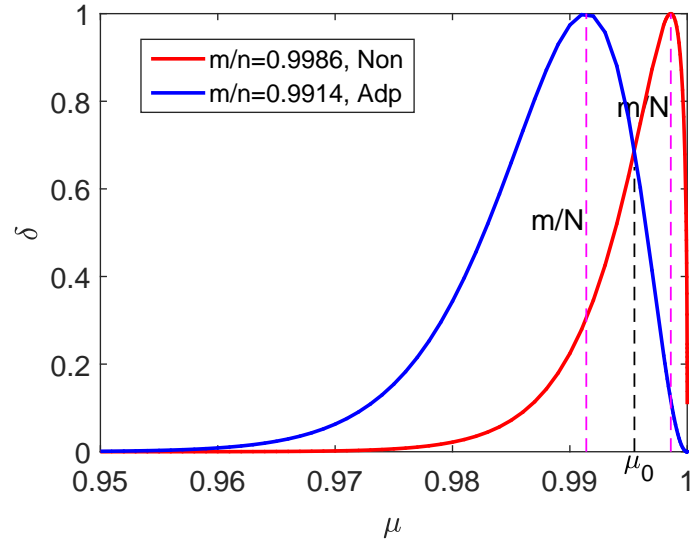
the variation of δ versus μ using equation $\delta = e^{-N D(m_{\text{pass}}/N \parallel \mu)}$, irrespective of the specific strategy. Therefore, the curves of nonadaptive and adaptive strategy coincide with each other in this situation. The expected probabilities μ_{Non} and μ_{Adp} are located at the different positions of the horizontal axis, as shown in the inset of Supplementary Figure 8. Note that $\mu \leq m_{\text{pass}}/N$ is for **Case 1** and $\mu \geq m_{\text{pass}}/N$ is for **Case 2** region when we choose different μ , i.e., $\epsilon (\mu = 1 - \Delta_\epsilon)$. From the figure we can see that the larger the difference between μ and m_{pass}/N , the smaller of the δ . This indicates that δ decreases more quickly for adaptive strategy in the **Case 1** region, whereas it decreases more quickly for nonadaptive strategy in the **Case 2** region.



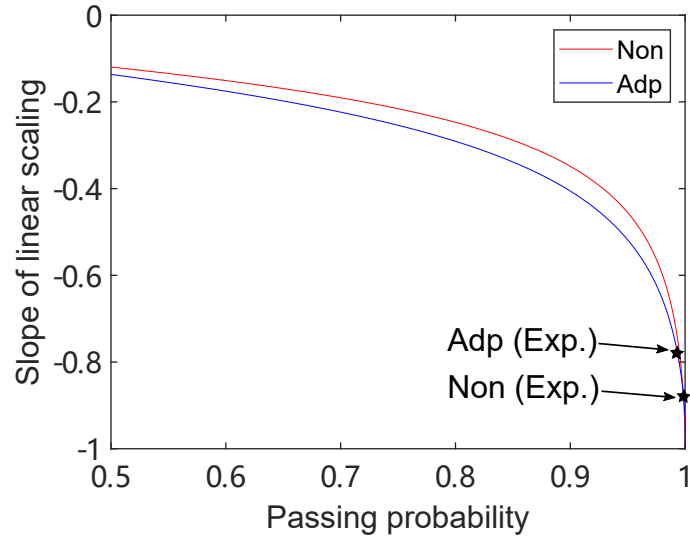
Supplementary Figure 8 The parameter δ changes with the anticipating passing probability μ when adopting the same m_{pass}/N . With the same ϵ , adaptive will always have a smaller μ than nonadaptive. Therefore, the adaptive will decrease faster than nonadaptive due to a larger difference in the $\mu \leq m_{\text{pass}}/N$ region. In the $\mu \geq m_{\text{pass}}/N$ region, the trend is opposite.

Second, we consider the situation where the nonadaptive and adaptive strategies have different passing probabilities m_{pass}/N , as in our experiment. For comparison, we adopt $m_{\text{pass}}/N = 0.9986$ for nonadaptive and $m_{\text{pass}}/N = 0.9914$ for adaptive based on our experimental data. The variation of δ versus μ is shown in Supplementary Figure 9. We can see that the comparison of nonadaptive and adaptive depends on the choice of μ . In the figure, we label the crosspoint of the two curves as μ_0 . If the ϵ is chosen such that both μ_{Non} and μ_{Adp} are smaller than μ_0 , the nonadaptive will drop faster than adaptive because nonadaptive has a smaller δ . On the contrary, if both μ_{Non} and μ_{Adp} are larger than μ_0 , the adaptive will drop faster than nonadaptive due to the smaller δ . If μ_{Non} and μ_{Adp} are located at two sides of μ_0 , the one which has a smaller δ in Supplementary Figure 9 will have a faster decline.

For ϵ versus the number of copies N , the scaling is determined by the passing probability m_{pass}/N , i.e., the fidelity of our generated states. The larger the passing probability, the faster the infidelity parameter ϵ decreases with the number of copies. For both nonadaptive and adaptive, ϵ will finally approach a asymptotic value. In Supplementary Figure 10, we plot the fitting slope of the linear scaling region versus the passing probability for both the nonadaptive and adaptive strategies. We can see that the adaptive strategy will have an advantage compared with nonadaptive strategy at a small passing probability. However, the slope tends to the optimal value -1 when the passing probability



Supplementary Figure 9 The parameter δ changes with the anticipating passing probability μ for different m_{pass}/N . In this situation, the one which adopts μ that results in a smaller δ will have a faster decline.



Supplementary Figure 10 The slope of linear scaling versus the passing probability. The slope decreases with the increase of the passing probability. Our experimental fitting slopes for the adaptive and nonadaptive strategies in the linear region is shown as the black stars. The slope approaches the optimal -1 when the passing probability are close 1. Due to the smaller passing probability of adaptive compared with nonadaptive, the absolute value of slope for adaptive strategy is also smaller. When the passing probability is large enough, the two strategies almost have an equal linear scaling slope at the same passing probability.

is large enough. This indicates that the optimal scaling can only be obtained at a high fidelity for the generated states. In the region of high fidelity, there is minor differences for the nonadaptive and adaptive strategies if we obtain a same passing probability. However, the adaptive strategy has a smaller passing probability than the nonadaptive strategy for our experimental data. Therefore, the descent speed of adaptive strategy is slower than the nonadaptive

strategy. This can be seen quantitatively from their fitting slopes -0.78 ± 0.07 (Adp) and -0.88 ± 0.03 (Non), shown as stars in Supplementary Figure 10.

Supplementary References

1. Pallister, S., Linden, N. & Montanaro, A. Optimal verification of entangled states with local measurements. *Phys. Rev. Lett.* **120**, 170502 (2018).
2. Wang, K. & Hayashi, M. Optimal verification of two-qubit pure states. *Phys. Rev. A* **100**, 032315 (2019).
3. Hayashi, M., Matsumoto, K. & Tsuda, Y. A study of LOCC-detection of a maximally entangled state using hypothesis testing. *J. Phys. A: Math. Gen.* **39**, 14427–14446 (2006).
4. During the optimization, we use the program offered by Kwiat Quantum Information Group. The code can be downloaded from their website. Last accessed: 2018-05-10.
5. Yu, X.-D., Shang, J. & Gühne, O. Optimal verification of general bipartite pure states. *npj Quantum Information* **5**, 112 (2019).
6. Dimić, A. & Dakić, B. Single-copy entanglement detection. *npj Quantum Information* **4**, 11 (2018).
7. Saggio, V. *et al.* Experimental few-copy multipartite entanglement detection. *Nature Phys.* **15**, 935–940 (2019).
8. Zhang, W.-H. *et al.* Experimental optimal verification of entangled states using local measurements. *Phys. Rev. Lett.* **125**, 030506 (2020).